# Coherent structures of $m = 1$ by low-Stokes-number particles suspended in a half-zone liquid bridge of high aspect ratio: Microgravity and terrestrial experiments

Tomoki Sakata,[*] Sayo Terasaki,[*] Hiroki Saito,[*] and Sorachi Fujimoto
*Division of Mechanical Engineering, School of Science and Technology, Tokyo University of Science, 2641 Yamazaki, Noda, Chiba 278-8510, Japan*

Ichiro Ueno[†]
*Department of Mechanical Engineering, Faculty of Science and Technology, Tokyo University of Science, 2641 Yamazaki, Noda, Chiba 278-8510, Japan*

Taishi Yano
*Department of Mechanical Engineering, Kanagawa University, 3-27-1 Rokkakubashi, Kanagawa-ku, Yokohama, Kanagawa 221-8686, Japan*

Koichi Nishino
*Department of Mechanical Engineering, Yokohama National University, 79-5 Tokiwadai, Hodogaya-ku, Yokohama, Kanagawa 240-8501, Japan*

Yasuhiro Kamotani
*Department of Mechanical and Aerospace Engineering, Case Western Reserve University, Cleveland, Ohio 44106-7222, USA*

Satoshi Matsumoto
*Japan Aerospace Exploration Agency, 2-1-1 Sengen, Tsukuba, Ibaraki 305-8505, Japan*

(Received 5 April 2021; accepted 4 January 2022; published 28 January 2022)

We investigate the coherent structures by low-Stokes-number particles suspended in half-zone liquid bridges of high Prandtl number via microgravity and terrestrial experiments. We especially focus on the structure by the suspended particle accumulation, or, the particle accumulation structure (PAS), of $m = 1$ in azimuthal wave number emerged in the traveling-wave-type time-dependent "oscillatory" convection. The particles form the closed path with a spiral structure in tall or high-aspect-ratio liquid bridges under both micro- and normal gravity conditions. Their formation process is evaluated by applying the accumulation measure, and it is indicated that the formation time of the structure is of the order of a thermal diffusion time regardless of the difference of Prandtl number as well as the gravitational acceleration. The spatial correlation between the coherent structure and the thermal wave over the free surface is illustrated in the rotating frame of reference. By the terrestrial experiments, we indicate how the PAS is conformed by the individual particle motions in the laboratory frame and the rotating frame of reference via two-dimensional particle tracking. We also indicate their occurring condition as a function of the slenderness

[*]These authors contributed equally to this work.
[†]ich@rs.tus.ac.jp

 

of the liquid bridges in terms of the volume ratio, and we evaluate the morphological characteristics of the spiral structure.

DOI: 10.1103/PhysRevFluids.7.014005

## I. INTRODUCTION

Coherent structures by tiny particles suspended in a closed geometry have attracted attentions after Schwabe *et al.* [1]. They found that tiny particles suspended as the tracers accumulate along a narrow path in thermocapillary half-zone liquid bridges of high Prandtl number Pr ($= \nu/\kappa$). Here $\nu$ and $\kappa$ are the kimenatic viscosity and the thermal diffusivity of the test liquid, respectively. Such accumulations, the particle accumulation structures (PAS) after Schwabe *et al.* [1], were found to emerge in the traveling-wave-type thermal flow regimes caused by so-called hydrothermal wave (HTW) instability in the high Pr liquid bridge [2] of finite height [3–6]. Here, the half-zone liquid bridge is a geometry in which a liquid is "bridged" between the coaxial cylindrical rods. This geometry has been widely employed in the fundamental studies to realize thermocapillary-driven convection by setting a designated temperature difference between the end surfaces of the rods. Then Tanaka *et al.* [7] indicated that the suspended particles gather along a closed structure with an azimuthal wave number $m$, which is the same as that of the HTW, and seem to rotate as a rigid body in the absolute coordinate, or, in the laboratory frame. They explored the emergence conditions of such unique structures as function of the intensity of thermocapillary effect and the liquid bridge shape in terms of the aspect ratio. It was examined that the PAS emerges in the liquid bridge beyond the threshold for the primary instability due to the HTW instability; namely, twice to four or five times larger than the threshold. The rigidity of the PAS in time as well as in space are achieved in a range of the thermocapillary-effect intensity up to the threshold for the secondary instability [8]. Tanaka *et al.* [7] indicated there exist two types of PAS by varying the intensity of the thermocapillary effect: spiral-loop (SL)1-PAS for lower intensity and SL2-PAS for higher intensity. SL1-PAS of $m$ consists of the fundamental structure called as the blades of $m$. SL2-PAS of $m$ also consists of the blades of $m$, whereas the tip region of each blade exhibits an additional loop [7,9,10]. The intensity of the thermocapillary effect in the energy transport is generally described by nondimensional Marangoni number defined as $\mathrm{Ma} = |\gamma_T|\Delta T L/(\rho\nu\kappa)$, where $\gamma_T = \partial\gamma/\partial T$ is the temperature coefficient of surface tension $\gamma$, $\Delta T$ is the temperature difference between the both ends of the liquid bridge, $L$ is the characteristic length, and $\rho$ is the density of the test liquid. As for the conditions in terms of the liquid-bridge shape, it has been known that the azimuthal wave number induced by the HTW instability depends on the aspect ratio $\Gamma = H/R$ [3,4,6], where $H$ and $R$ are the height and the radius of the liquid bridge, respectively, and also depends on the gravitational acceleration [11]. Schwabe *et al.* [12] conducted a sounding-rocket experiment and indicated that the dominant factor to realize PAS is not a gravitational acceleration, but the flow field induced by the thermocapillary effect.

Thus far knowledge on the PAS of $2 \leqslant m \leqslant 5$ has been accumulated extensively through the terrestrial experiments [7,9,10,13–18]; one has to prepare longer liquid bridge to produce smaller $m$ [3,4,7,19]. There exist difficulties to realize the PASs in high-aspect-ratio liquid bridges especially under normal gravitational acceleration [20]: To realize large Ma beyond the threshold of the primary instability to form the PAS, one has to increase $\Delta T$ and/or $H$, or has to decrease $\nu$. In the terrestrial experiment, there exists a severe limitation to increase $H$ because of the physical limitation to form the liquid bridge against static pressure. If one prepares the liquid bridge of small $H$ to realize small $m$, then one has to prepare the liquid bridge whose absolute size is small to keep high $\Gamma$. Thus one has to put large $\Delta T$ or has to prepare low viscous fluids, whereas one cannot avoid the evaporation of the test fluid. If one wants to realize the oscillatory convection in short liquid bridges for larger $m$ ($m \geqslant 5$), on the contrary, then one also has to increase $\Delta T$ to realize higher Ma despite of smaller characteristic length $L$. For both cases, then, the evaporation problem would become severer. These are the reasons why the previous research has focused on the PAS

with moderate $m$, which might be a reason why knowledge via numerical approaches has also been accumulated on the PAS of moderate $m$ [21–33].

There exist a few works dealing with PAS of $m \geqslant 5$ or $m = 1$ under the normal gravity condition; Yazawa and Kawamura [34] prepared two sets of the end disks whose diameters were of 10 and 20 mm, and realized the SL1-PAS of various $m$ up to 20 in the liquid bridges whose Pr is of 28 and 68. They also indicated there exists "double-mode" PAS, in which the PASs of $m = 2n$ and $m/2 = n$ emerge in the liquid bridge simultaneously. As for the PAS of $m = 1$, Sasaki *et al.* [35] realized them in the liquid bridge of Pr = 28, and found that two types of PAS of $m = 1$ exist by varying Ma. It must be noted that the PAS of $m \geqslant 2$ also exhibits two types by increasing Ma (SL1- and SL2-PASs [7]) as aforementioned, but the variation of the PAS of $m = 1$ is different from those: Sasaki *et al.* [35] showed that the particles form the closed path with a spiral structure in the interior region of the liquid bridge for the SL-PAS under lower Ma when one observes from above. Such a spiral structure corresponds to the helical motion of the particles following the return flow in the central region. When one increases Ma, the particles then form the closed path without such a spiral structure; this type of PAS realized at higher Ma exhibits a simpler structure. It seems opposite to the correlation for the SL1- and SL2-PASs of $m \geqslant 2$ against Ma. Schwabe *et al.* [12] also realized the SL-PAS of $m = 1$, but it is rather difficult to detect its whole spatial structure.

Recently the SL-PAS of $m = 1$ with a spiral structure was finely reproduced via the numerical simulation in the liquid bridges of Pr = 8 [36] and of Pr = 68 [37]. It must be noticed, however, that they reproduced the coherent structure only with the particles lighter than the test liquid, or, $\varrho = \rho_\mathrm{p}/\rho_\mathrm{l} < 1$, where $\rho_\mathrm{p}$ and $\rho_\mathrm{l}$ indicate the densities of the particles and the liquid, respectively. The terrestrial experiments [12,35] have revealed that the particles of $\varrho > 1$ realize the coherent structure of $m = 1$ as those of $m \geqslant 2$ [7,9,12,14,16–18]. As for the SL-PAS of $m = 1$ without a spiral structure, it was numerically reproduced with neutral-buoyancy particles [38,39] and with particles of various density [40]. It was also illustrated there is a PAS of $m = 1$ whose attracting orbit exhibits multiple revolutions under a certain condition [39,40].

Long-duration microgravity environment brings a significant benefit to overcome such difficulties to realize high Ma for high-$\Gamma$ liquid bridge of high Pr fluids. Because the static pressure becomes quite smaller than that under normal gravity, one can realize large and tall liquid bridge [11,41,42]. Thus, one would need smaller $\Delta T$ to realize large Ma than that on the ground. A Japan-US joint project so-called "Dynamic Surf" (principal investigator (PI): Yasuhiro Kamotani, one of the authors of this paper) had been conducted by use of the Fluid Physics Experiment Facility (FPEF) in the Japanese Experiment Module 'Kibo' on the International Space Station (ISS) during 2013–2016. This project was conducted successively after the project so-called "Marangoni experiments in space (MEIS)" [11,19,43–46]. After the five series of experiments of MEIS, three series of Dynamic Surf were conducted to investigate (a) correlation between the onset of the primary instability and the dynamic surface deformation of the free surface [47,48] and (b) effect of heat transfer through the free surface on the primary instability [49]. We have paid attention to the phenomena in liquid bridges of rather high Pr, or Pr > 65, with which it is quite difficult to conduct experiments under normal gravity condition. In addition to those primary objectives, we also paid close attention to realize the coherent structures in liquid bridges of such high Pr with larger $\Gamma$ by receiving benefits of long-duration and good microgravity conditions. As Matsumoto *et al.* [50] reported, coherent structures of $m = 2$ were realized in the liquid bridges of Pr = 112 and 207. Those coherent structures, however, were obtained in a transient state; that is, obtained in a period that the thermal boundary conditions in terms of $\Delta T$ or Ma were varying.

In addition to the occurring conditions for the PAS, we have another critical issue on the oscillatory convection in the tall liquid bridge: the selection of the convection type by the thermal flow field after the primary instability. Fukuda *et al.* [51] conducted series of terrestrial experiments and numerical simulations, and indicated that the standing-wave-type oscillation is rather dominant under the heat loss conditions for the high $\Gamma$ liquid bridges of high Pr in normal gravity. Especially for the liquid bridge of $\Gamma = 2.0$ and $V/V_0 \sim 1.0$ for Pr = 28.6, the traveling-wave-type oscillations emerge in a quite narrow range of the heat transfer between the test liquid and the ambient gas. They

also indicated that the PAS seldom emerges in the liquid bridge even in the traveling-wave-type oscillation. Similar characteristics were found in the microgravity experiments with tall liquid bridges of Pr $>$ 100 [46]. In other words, one has to explore severely the occurring conditions of the PAS when one changes the conditions and properties for the experiments. It is emphasized that Schwabe *et al.* [12] indicated that "the PAS for $m = 1$ is not easily observed because its existence range in $A$ '(aspect ratio)' and "in Ma is very narrow."

In this paper, we introduce coherent structures of $m = 1$ with a spiral structure produced successfully in a large-scale liquid bridge of high Pr in the Dynamic Surf. Those are the first examples to steadily realize the PAS of $m = 1$ under long-duration microgravity conditions. Correlations between the coherent structure and the thermal field over the free surface of the liquid bridge are discussed. We also introduce the coherent structures of $m = 1$ successfully obtained in the terrestrial experiments with a test liquid of Pr higher than that in Ref. [12]. Its formation process and spatial structure are discussed by considering the flow patterns induced by the HTW instability under different gravitational environments. Further, we illustrate how the PAS of $m = 1$ with a spiral structure is configurated by the individual particles via particle tracking technique.

## II. METHODS

The target geometry in this study is so-called half-zone liquid bridge. A designated amount of liquid is bridged between coaxial disks; the one end is heated and the other is cooled, then one can realize designated temperature difference $\Delta T$ between both ends of the liquid bridge to define the intensity of thermocapillary effect. Temperatures of the heated and cooled ends are maintained at $T = T_{\mathrm{H}}$ and $T_{\mathrm{C}}$, respectively, thus the temperature difference is defined as $\Delta T = T_{\mathrm{H}} - T_{\mathrm{C}}$. The radius of the disks is defined as $R$, and the distance between the disks or the height of the liquid bridge is defined as $H$. Throughout the present study, the characteristic length $L$ is defined by $1/L^2 = 1/H^2 + 1/R^2$ [11]. The shape of the liquid bridge is described with two parameters; the aspect ratio $\Gamma = H/R$ and the volume ratio $V/V_0$, where $V$ is the volume of the test liquid to form the liquid bridge itself and $V_0$ the volume of the straight cylinder formed between the disks or $V_0 = \pi R^2 H$. Apparatuses employed in the on-orbit and the terrestrial experiments are described in the following subsections.

### A. Microgravity experiments

We use the apparatus so-called "fluid physics experiment facility" (FPEF) installed in the payload rack of "Kibo" on the ISS for the series of the on-orbit experiments (Fig. 1). This facility employed in the Dynamic Surf was described in the previous reports [47–49]. In this paper, its essential parts are illustrated. This facility is designed to form a large-scale liquid bridge of high-Pr silicone oil. This consists of liquid-bridge formation system, temperature control system, exchangeable cassette of the test fluid, and measurement hardware. A series of experiments to quest the PAS were conducted within the third series of dynamic surf, "DS3." The series of DS3 were conducted for 30 days in total between the 17th November 2015 and the 30th November 2016. The heated disk is made of transparent sapphire. Its temperature is controlled by the indium tin oxide (ITO) film heater in a range between 20 and 90 °C. The cooled disk is made of aluminum. Its temperature is controlled in a range between 5 and 41 °C by the Peltier elements and cooling channel installed at the backside of the cooled disk. Temperatures of the heated and cooled disks are measured with two ITO film sensors and three K-type thermocouple sensors, respectively. We use a proportional-integral-derivative (PID) system to realize the precise temperature control; the resultant temperature stability is ±0.1 °C for both disks. In the third series of Dynamic Surf, the liquid bridge of $R = 15$ mm is utilized. The liquid-bridge shape in the present study to quest the PAS is kept as $\Gamma = 1.0$ and $V/V_0 = 0.95$, under which the oscillatory flows with $m = 1$ surely emerge [19]. Such condition was preliminary examined in this series of the DS3. Silicone oil of 10 cSt in kinematic viscosity $\nu$ (KF96L-10cs, Shin-Etsu Chemical Co., Ltd., Japan) is used as the test fluid to form the liquid

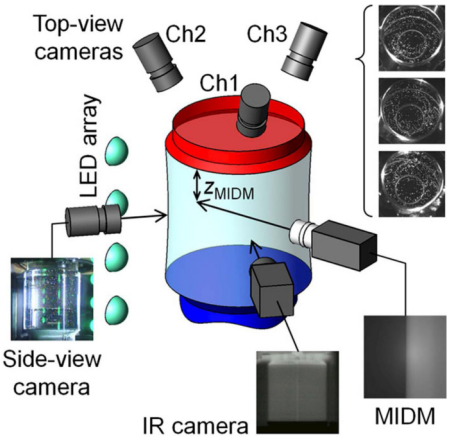


FIG. 1. Apparatus for microgravity experiment installed in the Japanese Experiment Module "Kibo" on the International Space Station (ISS) [47]. "Ch$i$" ($i = 1,\ 2,\ 3$) indicates the CCD camera of $i$th channel, and "MIDM" indicates the micro-imaging displacement meter.

bridge. Physical properties of the test liquids for on-orbit experiments are listed in Table I together with the ones for terrestrial experiments. Properties except $\gamma_T$ are given in Ref. [52]. The value of $\gamma_T$ was examined by the authors' group. Argon gas is installed in the chamber as the ambient gas at 94 kPa.

In the liquid bridge, gold-nickel-alloy coated acrylic particles are suspended as the tracer particles. The averaged diameter and density of the particle are of 180 μm and $1.30 \times 10^3$ kg/m$^3$, respectively. Their motions induced by the thermocapillary-driven convection in the liquid bridge are monitored via three black-and-white charge-coupled device (CCD) cameras ($720 \times 480$ pixels) mounted near the heated disk through the transparent sapphire. They are indicated as "Ch$i$" ($i = 1,\ 2,\ 3$) in the figure. Note that their incident angles to the end surface of the heated disk are inclined at about 13 deg against the central axis of the liquid bridge to apply three-dimensional particle tracking velocimetry (PTV) [53]. The camera parameters including the precise incident angles are obtained through the camera calibration processes. A color CCD camera ($720 \times 480$ pixels) is also installed to observe the liquid-bridge shapes and overall flow patterns via tracer particles from the side of the liquid bridge. The images captured by these cameras are downlinked through the image processing unit (IPU), which converts the images of $640 \times 480$ pixels. It is noted that the PTV technique was not applied for the series of experiments for the PAS because we put a larger number of particles inside the liquid bridge than that suitable for conducting the PTV, to realize a clear visualization of the PAS. The frame rate of the cameras are fixed at 30 frame per second (fps). The temperature of the liquid-bridge free surface is monitored at 30 fps via infrared camera ($320 \times 240$ pixels) with a temperature resolution of $\pm 0.2\,^\circ$C.

TABLE I. Physical properties of test fluids at 25 °C; 10-cSt silicone oil for microgravity experiments (DS3) and 2-cSt silicone oil for terrestrial experiments ($1g$).

| | $\nu$ [m$^2$/s] | $\rho$ [kg/m$^3$] | $\kappa$ [m$^2$/s] | $\gamma$ [N/m] | $\gamma_T$ [N/(m K)] | Pr |
|---|---|---|---|---|---|---|
| DS3 | $10.0 \times 10^{-6}$ | $9.35 \times 10^2$ | $8.81 \times 10^{-8}$ | $20.1 \times 10^{-3}$ | $-6.12 \times 10^{-5}$ | 113.5 |
| $1g$ | $2.0 \times 10^{-6}$ | $8.73 \times 10^2$ | $7.00 \times 10^{-8}$ | $18.3 \times 10^{-3}$ | $-7 \times 10^{-5}$ | 28.6 |

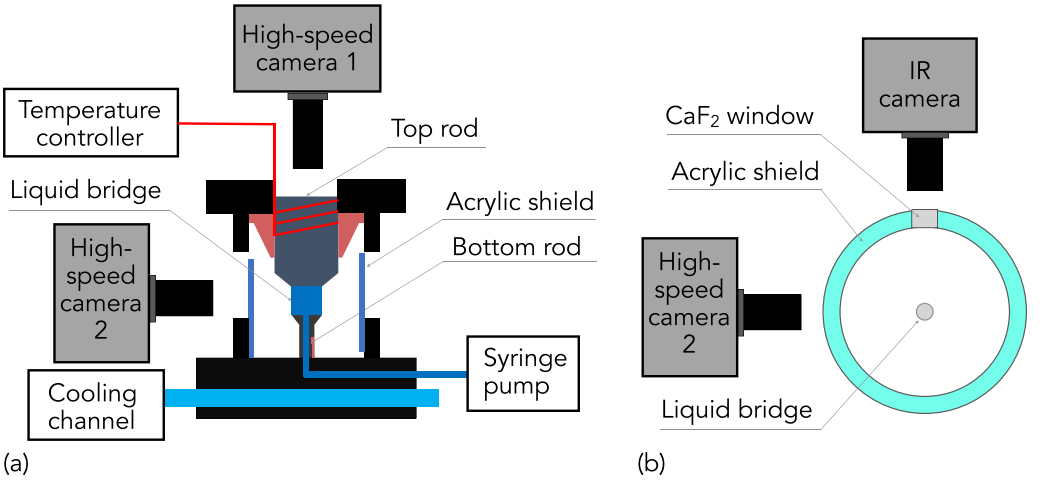


FIG. 2. Apparatus for terrestrial experiment.

### B. Terrestrial experiments

To overcome the significant effect of static pressure under normal gravity condition, we employ small-size liquid bridge in the terrestrial experiments. Figure 2 illustrates the schematics. The apparatus consists of two major parts; the one for sustaining the liquid bridge, and the other for accumulating the data of the particles images and temperatures in the system. Almost of all apparatus are the same as described in Ref. [51].

The liquid-bridge sustaining part for the terrestrial experiments also consists of the top and bottom rods whose end surfaces are the coaxial circles. The radius of the both end surfaces is of 0.75 mm. The top rod is made of transparent sapphire, and is heated at the designated temperature $T_{\mathrm{H}}$ by a heater of a nichrome wire wound around the rod. The temperature of the top rod is monitored by K-type thermocouple embedded in the rod. The heater and the thermocouple are connected to the temperature controller (Model 335 Cryogenic Temperature Controller, Lake Shore Cryotronics Inc., USA) to adjust the top-rod temperature by the PID control. The bottom rod is made of aluminum, whose radius of the end surface is the same as that of the top-rod end surface. To prevent undesignated liquid dripping from the bottom rod, the upper edge of the bottom rod is tapered at 45 deg, and is coated with fluorine. A hole of 0.15 mm in radius is drilled through along the center of the bottom rod, which is connected to the syringe filled with the test liquid via a tube. From the syringe controlled by the syringe pump, the test liquid is supplied through the hole. The temperature of the bottom rod is kept at $T_{\mathrm{C}} = 20\,^{\circ}\mathrm{C}$ by using a cooling channel through its base block. A designated temperature difference $\Delta T = T_{\mathrm{H}} - T_{\mathrm{C}}$ is realized by heating the top rod. The liquid-bridge shapes in the terrestrial experiments are kept as $\Gamma = 2.0$ but varying $V/V_0$ in a range of $0.6 \leqslant V/V_0 \leqslant 1.0$, under which the oscillatory flows of $m = 1$ are surely emerged. It was indicated that the condition of $\Gamma = 2.0$ and $V/V_0 = 1$ brought a stable formation of PAS of $m = 1$ for $n$-decane [12], but not for the present test liquid (2-cSt silicone oil) [51].

The liquid bridge is concentrically surrounded by a acrylic shield of 7.5 mm in inner diameter and of 3 mm in thickness to fix the thermal boundary conditions around the liquid bridge as much as possible; this shield prevents undesignated buoyant flows of the ambient gas realized in the open system [17,18]. A $CaF_2$ window (2 mm in width, 6 mm in height, and 3 mm in thickness) is installed at a tiny part in the azimuthal direction of the shield, which allows us to monitor the surface temperature via an infrared (IR) camera (Thermography R300, NEC Avio Infrared Technologies Co., Ltd., Japan) with a closeup lens (TVC-2100UB, NEC Avio Infrared Technologies Co., Ltd., Japan). We record the IR images of $320 \times 240$ pixels at a fixed frame rate of 60 fps under a

temperature resolution of 0.05 K at 30 °C. The sensor of this IR camera detects the infrared light in a range of 8 μm to 14 μm in wavelength. The absorption coefficient as the optical property of our own silicone oil is unfortunately unknown, so the IR images do not indicate actual value of the free-surface temperature as described in Ref. [54]. In this work, we call this qualitative variation as "temperature" for the sake of brevity as conducted in Refs. [18,54].

In this system, the successive images of the particles suspended in the liquid bridge are captured by two synchronized high-speed complementary metal-oxide semiconductor (CMOS) cameras of $2048 \times 2048$ pixels at frame rates up to 500 fps (FASTCAM-Mini WX100, Photron, Inc., Japan); the one from above through the transparent top rod, and the other from the side through the external shield. The alignment of the high-speed camera for the side view and the IR camera is the same as Gotoda *et al.* [17]. That is, the IR camera is placed at the position of $\pi/2$ apart from the side-view camera. In the previous research [10,16,17], the phase correlation between the PAS and the thermal-flow field was examined by monitoring the temperature variation over the free surface via the IR camera and the particles motion through the transparent top rod via the high-speed camera for the oscillatory flow of $m = 3$. We reconstruct the particle positions against the traveling-wave thermal-flow field with the same protocol as conducted in Refs. [17,18], and obtain the particle positions in the rotating frame of reference as follows: We record the images by the high-speed cameras for top- and side views as well as the IR camera simultaneously. We measure the fundamental frequency of the PAS and the surface temperature deviation independently from both data by the high-speed camera for the top view and the IR camera. Under the present conditions, the fundamental frequency of the traveling-wave-type oscillatory convection becomes constant during the observation period. Thus the phase difference among the data obtained by the top-view camera, the side-view camera, and the IR camera is constant. Note that it has been known that the fundamental frequency of the rotating motion of the PAS and that of the traveling wave of the thermal-flow field are identical [17,18]. The synchronization between the data by the high-speed and IR cameras is achieved by delaying the phase of the data by the IR camera based on the period that takes to rotate the PAS in $\pm 90$ deg depending on the azimuthal direction of the PAS rotation. The images in the rotating frame of reference are drawn by accumulating the images after the rotation following the HTW [17,55]: Suppose the HTW rotates azimuthally at angular velocity $\omega$, and one has a series of original particle images in the laboratory frame $\mathcal{I}(t)$, where $t$ is the time elapsed. One obtains the image $\mathcal{I}'(t)$ by rotating $\mathcal{I}(t)$ in $(-\omega t)$ in the azimuthal direction around the liquid-bridge center. The integrated particle images $\sum \mathcal{I}'(t)$ is the image in the rotating frame of reference.

The shape of the liquid bridge is monitored through the shield to confirm its volume ratio $V/V_0$. The volume ratio is kept constant as designated by supplying the test liquid through the drilled hole in the bottom rod via the syringe pump to prevent any changes in the volume ratio due to evaporation as aforementioned. The velocity of the injected liquid is less than $3.0 \times 10^{-6}$ m/s, which is significantly smaller than that of the thermocapillary-driven convection; the supply of the test liquid is conducted at a minimum rate as small as possible to avoid significant disturbances to the flow field by injection as discussed in Ref. [18].

The test liquid for the terrestrial experiments is 2-cSt silicone oil (KF96L-2cs, Shin-Etsu Chemical Co., Ltd., Japan), whose Prandtl number is of 28.6 at 25 °C. The physical properties of the test fluid are listed in Table I. Gold-nickel-alloy coated acrylic particles (MX-1000NA, Soken Chemical and Engineering Co. Ltd., Japan) are employed as the test particles. The diameter and density of this particle are of 10.5 μm and $2.06 \times 10^3$ kg/m$^3$, respectively.

### C. Common information and processes for both of experiments

#### *1. Gravity effects*

The effects of gravity on the liquid bridge shape and the thermal-flow fields are examined by considering the static and dynamic Bond numbers defined as $\mathrm{Bo} = \rho g H^2/\gamma_0$ and $\mathrm{Bd} = \rho g \beta H^2/|\gamma_T|$, respectively, where $g$ is the gravitational acceleration, $\gamma_0$ is the characteristic surface tension, and $\beta$ is the thermal expansion coefficient. In the present study, the static Bond numbers become

$\mathrm{Bo}_{\mathrm{DS3}} = 1.0 \times 10^{-2}$ and $\mathrm{Bo}_{1g} = 1.1$, and the dynamic Bond numbers become $\mathrm{Bd}_{\mathrm{DS3}} = 3.6 \times 10^{-3}$ and $\mathrm{Bd}_{1g} = 0.34$. Here the subscripts DS3 and $1g$ denote the on-orbit and terrestrial experiments, respectively. For the on-orbit experiment, the gravitational acceleration is characterized as $10 \times 10^{-6} \lesssim g/g_0 \lesssim 10 \times 10^{-4}$ [56], where $g_0 = 9.81\,\mathrm{m}/s^2$. In evaluating $\mathrm{Bo}_{\mathrm{DS3}}$ and $\mathrm{Bd}_{\mathrm{DS3}}$, $g = 10^{-4} g_0$ is used as the typical value for the gravitational acceleration. The characteristic surface tension $\gamma_0$ is defined as $\gamma$ at 25 °C. It must be reminded that we do not obtain a condition of $\mathrm{Bo} = \mathrm{Bd} = 0$ even in the on-orbit experiments.

#### *2. Evaluation of* Ma *and* $\epsilon$

To evaluate Ma, the mean value of $\nu$ for $T_{\mathrm{H}}$ and $T_{\mathrm{C}}$ is adopted as the characteristic viscosity (i.e., $\nu = \{\nu(T_{\mathrm{H}}) + \nu(T_{\mathrm{C}})\}/2$). The temperature dependence of the kinematic viscosity is considered by using an empirical correlation [52] as $\nu(T)/\nu_0 = \exp\{5.892(25 - T)/(273.15 + T)\}$, where $\nu_0$ is the kinematic viscosity of the test liquid at 25 °C, and $T$ is the temperature in Celsius. The other properties are almost constant in the temperature range of the present experiment. As for the microgravity experiments, we obtained the critical Ma for the primary instability, $\mathrm{Ma}_{\mathrm{c}}^{(1)}$, under the present condition [47,49]. We thus evaluate the distance in Ma from the onset condition of the oscillatory convection as $\epsilon = (\mathrm{Ma} - \mathrm{Ma}_{\mathrm{c}}^{(1)})/\mathrm{Ma}_{\mathrm{c}}^{(1)}$ [57].

#### *3. Waiting time for thermal-flow fields in experiments*

After monitoring the thermal-flow fields and the particles' behaviors for a certain Ma, we change the power input to the heaters installed in the top rod to vary $\Delta T$ and Ma. The variation of $\Delta T$ for a single step is small enough not to affect the flow transition [58]. After a waiting period of at least a few thermal diffusion times for the microgravity experiments and ten thermal diffusion times for the terrestrial experiments to develop the thermal-flow field, we then start recording procedures for the particles' behaviors and the surface temperature. Here we define the thermal diffusion time $\tau := L^2/\kappa$; $\tau$ for DS3 and $1g$ are $\tau_{\mathrm{DS3}} = 1.28 \times 10^3$ s and $\tau_{1g} = 6.43$ s, respectively. Note that the waiting time in the microgravity experiments is inevitably much shorter in terms of the thermal diffusion time than that for the terrestrial experiments. This is due to the severe limitation of the operation time for the microgravity experiments; we were normally supposed to conduct the experiment during the crew sleeping time 21 : 30 − 06 : 00 in GMT [or 06 : 30 − 15 : 00 in JST (the Japan Standard Time)], including the formation and the restore of the liquid bridge after the cooling process of the test liquid.

#### *4. Particle properties*

The Stokes number of the particles concerned is evaluated by the definition as $\mathrm{St} = \varrho d_{\mathrm{p}}^2/(18H^2)$ [59], where $\varrho$ is the density ratio between the particle $\rho_{\mathrm{p}}$ and the test liquid $\rho_{\mathrm{l}}$ or $\varrho = \rho_{\mathrm{p}}/\rho_{\mathrm{l}}$, and $d_{\mathrm{p}}$ is the particle diameter. In the present study, those values of our particles are $\mathrm{St}_{\mathrm{DS3}} = 1.1 \times 10^{-5}$ and $\mathrm{St}_{1g} = 6.4 \times 10^{-6}$. Note that the density ratio $\varrho$ for the on-orbit and terrestrial experiments are both less than unity.

## III. RESULTS AND DISCUSSION

### A. Microgravity experiment

On December 10, 2015 (GMT), we conducted an experimental run in the "Kibo" aboard the ISS to quest the formation condition of the particle accumulation structures under high $T_{\mathrm{C}}$ to enlarge a heat loss condition. Figure 3 illustrates (1) the series of the snapshots of the particle images taken by one of the top cameras and (2) corresponding variation of the accumulation measure $K(t)$ originally proposed by Kuhlmann and Muldoon [24]. This measure indicates the process of the accumulation of the suspended particles quantitatively. In the present study we employ the process in Refs. [10,16] to evaluate this measure from the particle images obtained through the top rod: We consider a square of $2R$ in side lengths as a monitoring area. The area is divided into $50 \times 50$

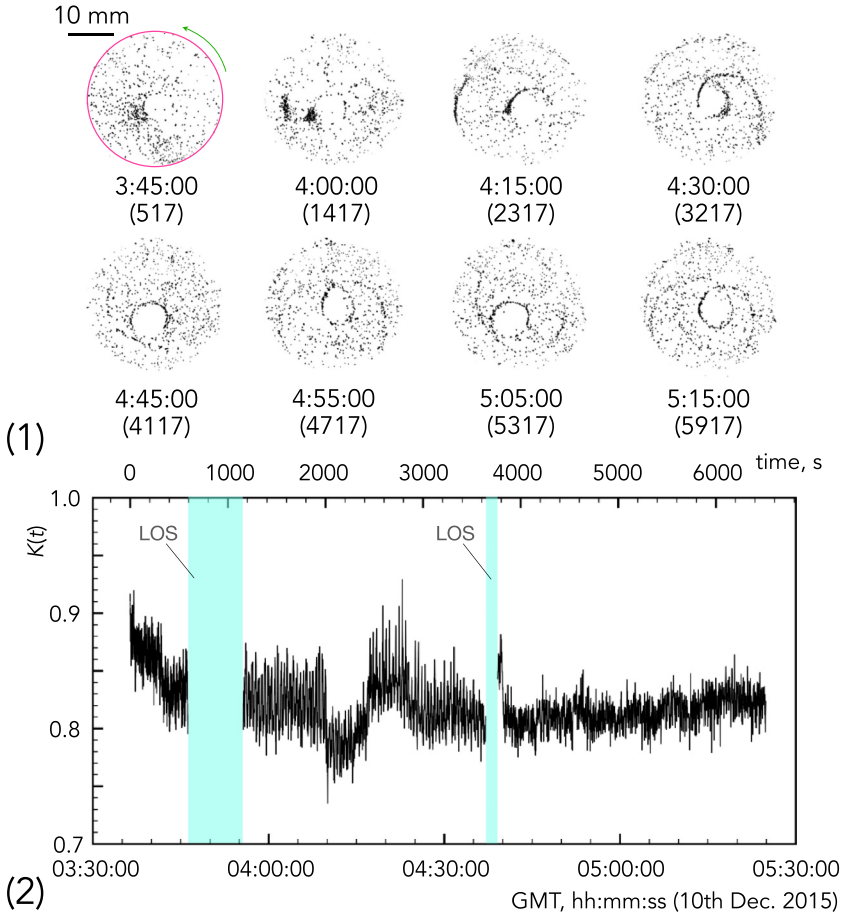


FIG. 3. (1) Variations of top view of the particle images, and (2) corresponding $K$ measure under $\mathrm{Ma} = 1.30 \times 10^4$ ($\Delta T = 8.2$ K and $\epsilon = 0.8$) in liquid bridge of $V/V_0 = 0.95$ and $\Gamma = 1.0$ under microgravity condition. In the first frame in panel (1), the periphery of the top disk (circle) and the azimuthal propagation direction of the traveling-wave-type oscillation (arrow) are illustrated. Time in GMT (and the elapsed time in second) is indicated in panel (1). "LOS" in panel (2) is the abbreviation for "loss of signal" from the International Space Station. More detailed time series of the particle images is illustrated in Fig. 11(a) in Appendix A.

cells. Each cell consists of $10.3 \times 10.3$ pixels. The monitoring area thus includes the outer region of the liquid bridge, where no particles appear, as employed in the previous research [10,16]; this is a different point from Kuhlmann and Muldoon [24]. The accumulation measure $K(t)$ is defined as $K(t) = \{2(N_\mathrm{p} - \overline{N})\}^{-1} \Sigma_{i=1}^{N_\mathrm{cells}} |N_i(t) - \overline{N}|$, where $N_\mathrm{p}$ is the number of the particle pixels, $\overline{N}$ is the average number of the particle pixels in each cell, $N_i(t)$ is the number of the particle pixels in the $i$th cell at time $t$, and $N_\mathrm{cells}$ is the total number of the cells. Note, as discussed in Ref. [10], that $N_\mathrm{p}$ is hardly constant within the measuring period in the experiments. This is because the particles are counted in the projected images, and there exist some particles uncountable due to the overlapping. We changed $T_\mathrm{H}$ from 45.3 °C to 48.2 °C at GMT 03 : 36 while kept $T_\mathrm{C}$ at 40 °C, and then we waited for developing the thermal flow field. During the waiting period, we observed that the particles form a "bunch" [1] in the central region around the particles depletion zone (GMT 03 : 36 : 23 − 04 : 10 : 06). At around GMT 04 : 20 : 00, the particles formed a coherent structure, resulting in the increase of $K(t)$. After the LOS (loss of signal) for about 550 s, we added

the liquid of 0.15 cc at 0.005 cc/s to adjust the liquid-bridge volume ratio from 0.93 to 0.95 at around GMT 04 : 40 : 23. A spike in $K(t)$ after the volume adjustment is due to a noise in the particle image; a reflection of the light by the disk edge results in the increase of the bright pixels to be counted. One can thus ignore this sharp variation in $K(t)$. We then confirmed a coherent structure of $m = 1$ with a spiral structure stably for more than 40 min. Note that it is impossible to evaluate the precise formation time of the PAS from the variation of $K(t)$ because we did not have any equipments in the apparatus nor conduct any procedures to disperse the suspended particles in the liquid bridge as conducted in the ground experiments [10,13,14,16]. Through the present observation in the microgravity experiments, however, it seems for the particles to take about at least $1 \times 10^3$ s$-1.5 \times 10^3$ s or about a thermal diffusion time to form a coherent structure. This confirms for the first time that the formation time is of the order of the thermal diffusion time as indicated by the ground experiments [10,16]. Behaviors of the PAS of $m = 1$ with a spiral structure realized under microgravity are illustrated in Fig. 4; the temporal variations of the snapshots of the particle images observed (a) from above and (b) from side, and (c) the surface temperature deviation obtained by the IR camera. The particle images are indicated after the inversion of the gray scale; the black dots correspond to the particles suspended in the liquid bridge. The volume ratio of the suspended particles to the liquid bridge is evaluated as about 0.2 %. This structure emerges under $\mathrm{Ma} = 1.30 \times 10^4$ ($\Delta T = 8.2$ K, $\epsilon = 0.18$) in the liquid bridge of $V/V_0 = 0.95$ for $\Gamma = 1.0$. The fundamental frequency of the HTW, or, that of the PAS rotation, is evaluated as 0.030 Hz. Thus the characteristic period of the PAS formation ($1 \times 10^3$ s $\sim 1.5 \times 10^3$ s) is found to be about 30∼45 periods of the PAS rotation. This agrees well with the values obtained in the previous research [13,60]. The occurrence condition in $\epsilon$ is surprisingly smaller than that for the PAS of $m = 3$ [7,12]. Schematic of the trajectory of the particles forming the coherent structure is illustrated in the first panel superimposed on the same images as indicated in (i). This schematics is obtained by integrating the particle images in the rotating frame of reference as conducted in Refs. [10,17,18,55]. The point "A" indicates the position of the trajectory where the coherent structure locating closest to the free surface near the heated disk. The particles travel along the positions on the trajectory in the alphabetical order; when one pays their attention to the particles forming the PAS, they exhibit clockwise motion in net in this case. That is, the net azimuthal direction of the particles motion along the PAS is opposite to that of the HTW as indicated for the PAS of $m = 3$ [7,9,13,14,18]. What we realized in the large-scale liquid bridge under microgravity has a similar structure to that in the ground experiment [35]. After sliding near the free surface toward the cold disk (from the position "A" to "B"), the particles penetrate into the central region of the liquid bridge (from "B" to "C"). Note that the schematic trajectory between the positions "A" and "B" is illustrated with the dashed line because the particles traveling near the free surface are not successfully obtained due to their fast motion. There exists a particle depletion zone in an almost circular shape, which rotates around the center axis of the liquid bridge. The particles start rising toward the heated disk around the particle depletion zone by varying the azimuthal position about $2\pi$ (along "C," "D," "E," and "F"), and move toward the free surface near the hot disk (from "F" to "A"). Such trajectory with a helical shape was observed in the ground experiment in the liquid bridge of $\mathrm{Pr} = 15$ [35] but was not apparently observed in the liquid bridge of $\mathrm{Pr} = 8$ and $\Gamma \sim 2.0$ [12]. It is noted that the preferable $\Gamma$ of the liquid bridge for the oscillatory convection with a certain $m$ becomes lower in the microgravity condition than that in the normal gravity [19]. The present results by the on-orbit experiment follows what have been found in the previous research. That is, the PAS of $m = 1$ is realized in the liquid bridge of $\Gamma = 1.0$ in the microgravity, although in the liquid bridge of $\Gamma > 1$ in the normal gravity (e.g., $\Gamma = 2.0$ in Refs. [12,35]).

The particle images in the absolute coordinate clearly indicate that some amount of the suspended particles accumulate along a winding structure as observed experimentally [35] and numerically [36]. This coherent structure seems rotating at a constant angular velocity in counter-clockwise direction. This angular velocity almost match to that of the thermal wave over the free surface as shown in row (c). The time series in this figure are illustrated in terms of the phase of the rotation. It should be noted that the distribution of $\widehat{T}$ apparently seems different at 0 and $2\pi$ in phase; this is

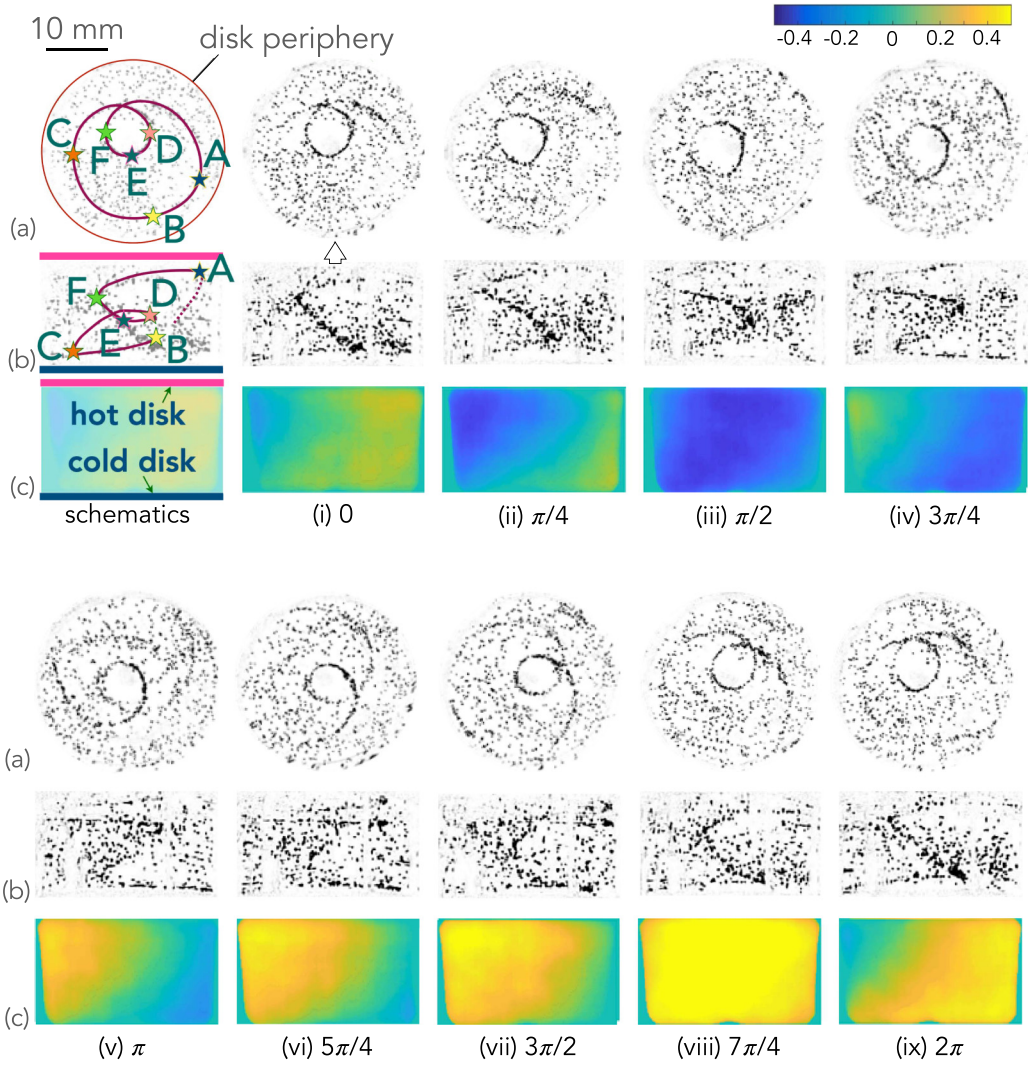


FIG. 4. Temporal variations of (a) top view and (b) side view of the particle images, and (c) surface temperature deviation obtained by microgravity experiment: $\mathrm{Ma} = 1.30 \times 10^4$ ($\Delta T = 8.2\,\mathrm{K}$ and $\epsilon = 0.18$), and $V/V_0 = 0.95$ for $\Gamma = 1.0$. Schematic of the trajectory of the particles forming the coherent structure is illustrated in the first panel superimposed on the same images indicated in (i). The point "A" indicates the position of the trajectory where the coherent structure locating closest to the free surface near the heated disk. The particles travel along the positions on the trajectory in the alphabetical order.

because we could not have enough waiting period to develop the thermal-flow field in the present on-orbit experiments as aforementioned. As indicated in the following subsection as well as in the previous research [10,17,18], the propagation of the thermal wave over the free surface and the coherent structure would perfectly match if one has long enough waiting period. One finds a pair of positive and negative $\widehat{T}$ propagating in counter-clockwise direction at a constant speed. If one pays attention to the negative $\widehat{T}$, it forms a bandlike structure inclined against the $z$ axis. This is a typical feature of the thermal wave induced by the HTW instability in high Pr fluids as seen in the liquid bridges [10,17,44,46,61–63], in the liquid films [64–66], and in the hanging droplets [54,67]. The angle of inclination seems almost constant along the $z$ axis; the thermal wave seems propagating

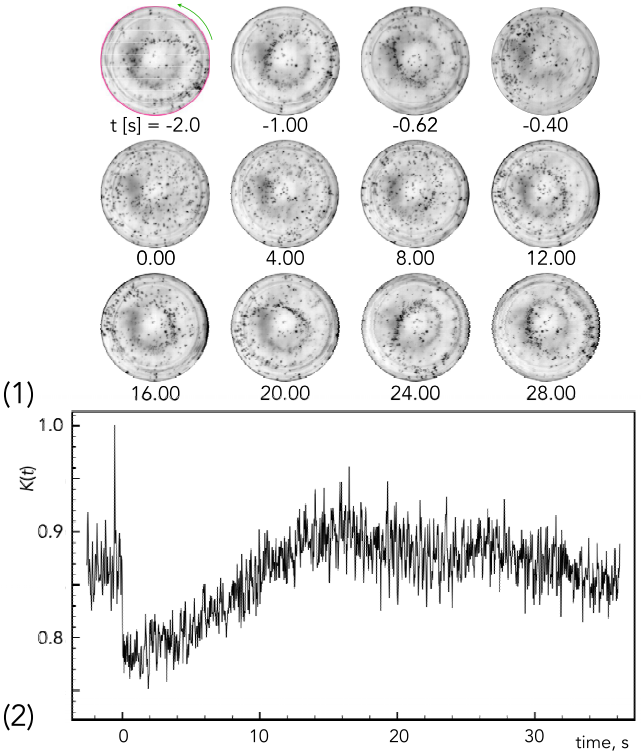


FIG. 5. (1) Variations of top view of the particle images, and (2) corresponding $K$ measure by terrestrial experiment; $\mathrm{Ma} = 1.9 \times 10^4$ ($\Delta T = 20\,\mathrm{K}$) for $V/V_0 = 0.8$ and $\Gamma = 2.0$. At $t = -1.1\,\mathrm{s}$ a disturbance to the free surface is put by blowing a tiny amount of the air through the external shield, and at $t = 0$ the disturbance to the liquid bridge is stopped. Note that the azimuthal direction of rotation before adding the disturbance is counterclockwise as indicated by an arrow in the first frame in (1), and that after adding the disturbance becomes clockwise. More detailed time series is illustrated in Fig. 11(b) in Appendix A.

from the heated disk to the cooled disk with a constant incident angle. It has been known that the propagation angle depents on Pr [64]. Such thermal waves emerge in the thermal flow fields of HTW(a′) and HTW(a) as indicated via linear stability analysis [68] (see Appendix B).

### B. Terrestrial experiment

Figure 5 illustrates a typical example of the formation process of the PAS of $m = 1$ with a spiral structure in the liquid bridge of $\Gamma = 2.0$ under the normal gravity condition. The volume ratio of the suspended particles to the liquid bridge is evaluated as about 0.02 %. This structure emerges under $\mathrm{Ma} = 1.9 \times 10^4$ ($\Delta T = 20\,\mathrm{K}$) for $V/V_0 = 0.8$. The fundamental frequency of the HTW is of 2.63 Hz. It was found that the existence range of the PAS of $m = 1$ in terms of Ma is quite narrower comparing to those for $m \geqslant 2$ [12], and that the PAS seldom emerges in the liquid bridge of $\Gamma = 2.0$ and $V/V_0 \sim 1.0$ in the present system [51] as indicated in Sec. I, so that we quested the occurring condition by varying $V/V_0$ in the preliminary experiments.

Panel (1) indicates the snapshots of the top-view particle images, and panel (2) illustrates the corresponding $K(t)$. In this experimental run, the PAS of $m = 1$ with a spiral structure is once fully established until $t < -1.1\,\mathrm{s}$. At $t = -1.1\,\mathrm{s}$ we put a disturbance to the free surface by blowing a tiny amount of the air through the external shield; we use a syringe to blow the air, whose needle is installed through a hole prepared on the external shield. Right after the adding the disturbance, the

particles forming the PAS scatter from the coherent structure, and thus $K(t)$ exhibits an abrupt drop. Blowing the air to the free surface corresponds to the local varying of the heat transfer condition between the liquid bridge and the ambient gas. The thermal-flow field is affected by the heat transfer, and the preferable thermal-flow field changes [51,69]. This is why the PAS disappears by adding such disturbance. We then stop blowing at $t = 0$ s. It is noted that the rotating direction of the HTW becomes opposite to that before adding the disturbance; from the counterclockwise to the clockwise. This is a sign that the thermal-flow field is once significantly destroyed by the disturbance and then reform the traveling-wave-type oscillatory state. One cannot predict the rotating direction after adding the disturbance. Slightly after the end of the disturbance, $K(t)$ reaches the minimum and increases as time elapses. Accompanying the progress of the coherent-structure development, $K(t)$ increases monotonically, and reaches the maximum at around $t = 16$ s. The period $\Delta t \sim 16$ s corresponds to about 2.5 thermal diffusion time. One can reproduce the formation of the PAS under this condition, and finds that the spatial structure of the PAS and the formation time are identical independently of the initial conditions. It is found that the formation time for the PAS of $m = 1$ with a spiral structure is rather longer than that for the PAS of $m = 3$ (about 1 to 1.5 thermal diffusion time) [16], although it is hard to measure the actual formation time of the coherent structure by the experiments because it is rather impossible to disturb only the particles' behaviors without disturbing the thermal flow field [10]. It is also found that the order of the formation time of the PAS of $m = 1$ with a spiral structure observed in the microgravity experiment agrees well with that in the terrestrial experiments. In addition, this formation time corresponds to about 42 periods of the PAS rotation, which also agrees with the values by the previous research for various $m$ [13,60] and the present microgravity experiment. These are the first data for the formation time of the PAS of $m = 1$ with a spiral structure in the different gravitational acceleration and for the liquids of different Pr. We do not reach any concluding ideas, however, to predict the formation time and its dependencies on the particle size and density [12], the fluid properties such as Pr, the shape of the liquid bridge, and so on. Further investigation would be indispensable to lead comprehensive conclusions via high-resolution simulations as well as fine terrestrial/microgravity experiments.

Figure 6 illustrates the temporal variations of the snapshots of the inverted particle images by the terrestrial experiments observed (a) from above and (b) from side, and (c) the surface temperature deviation obtained by the IR camera. Note that this result was obtained in the different experimental run shown in Fig. 5. The PAS seems rotating in the counter-clockwise direction, and the particles travel azimuthally in the clockwise direction in net, which is identical to the result in the microgravity experiment as introduced. As conducted in Fig. 4, we illustrate the schematic of the trajectory of the particles forming the coherent structure in the first panel superimposed on the same images indicated in (i); the point "A" indicates the position of the trajectory where the coherent structure locating closest to the free surface near the heated disk, and the particles travel along the positions on the trajectory in the alphabetical order. The trajectory of the particles forming the PAS is quite similar to that as shown in Fig. 4; when the particles rise in the central region of the liquid bridge they exhibit a helical motion around the particle depletion zone. Note that the size of the particle depletion zone against the liquid bridge diameter in the terrestrial experiment is greater than that in the microgravity experiment. This difference might come from the difference of the thermal flow field induced by the HTW instability, which is judged by monitoring (c) the surface temperature deviation. There exist a pair of positive and negative $\tilde{T}$ propagating in counter-clockwise direction at a constant speed, as seen in Fig. 4 (3). The propagation direction of the thermal wave, on the contrary, is almost normal to the both end disks. This is a typical feature of the propagating thermal wave in the thermal flow field of the HTW(b) (see Appendix B); the linear stability analysis indicates that the thermal flow field of the HTW(b) emerges in the liquid bridge of $\Gamma = 2.0$ under Bi $\sim 0$ for Pr $= 28.6$ and Bd $= \mathcal{O}(0.1)$ [68] but never emerges for Bd $= 0$. It is noted that the thermal flow field of the HTW(b) was also realized in the microgravity experiment with the liquid bridge of Pr $= 112$, $\Gamma = 3.0$, and $V/V_0 = 0.95$ [49]; one finds the HTW(b) dominates under $T_C = 15\,^\circ$C (or, lower Bi), whereas finds the HTW(a) or HTW(a′) under $T_C = 20\,^\circ$C (or, higher Bi) [49]. It is reasonable to realize the PAS of $m = 1$ with the thermal flow field of the HTW(b) in the terrestrial experiment

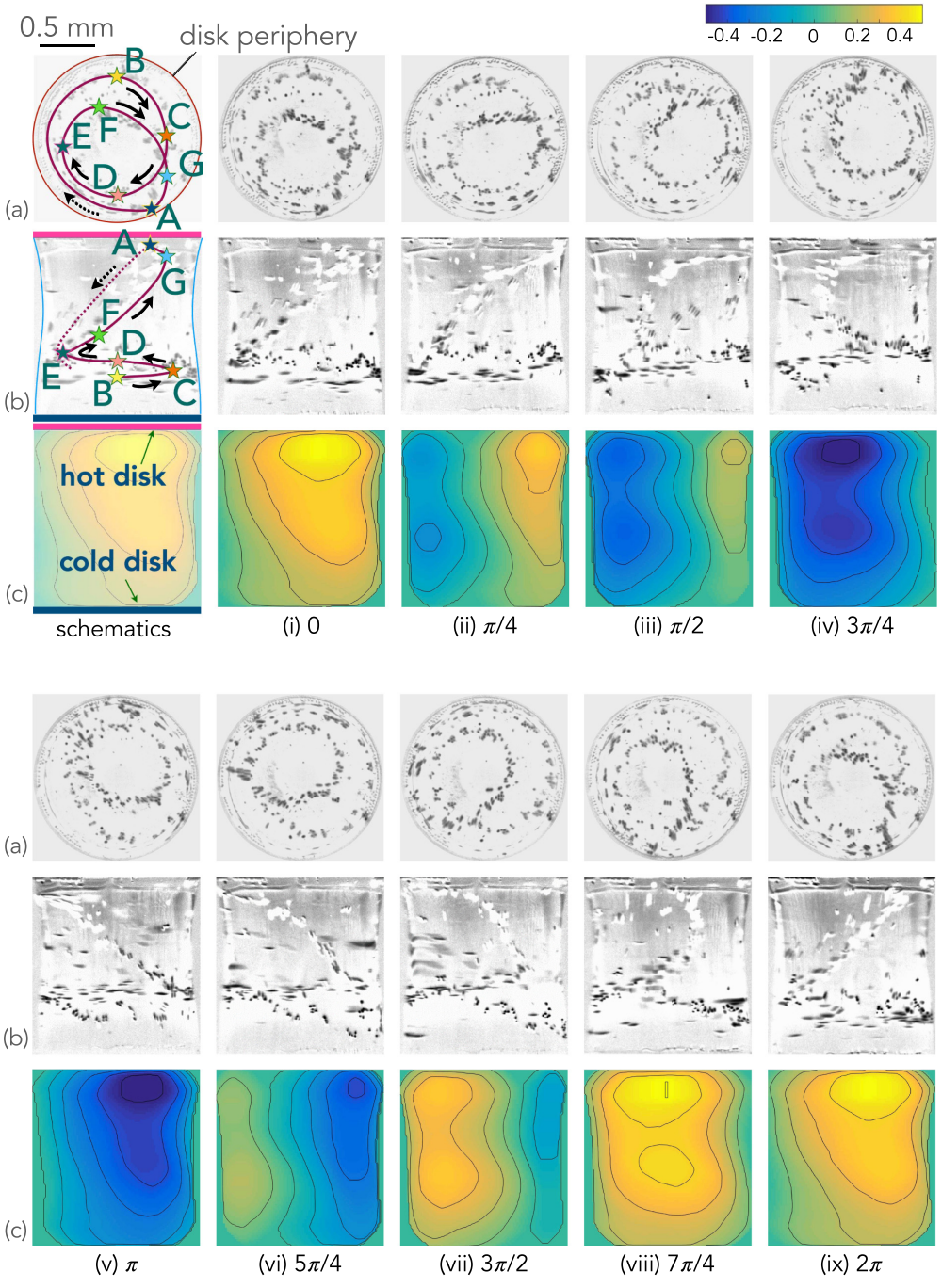


FIG. 6. Temporal variations of (a) top view and (b) side view of particle images, and (c) surface temperature deviation obtained by terrestrial experiment: $\mathrm{Ma} = 1.9 \times 10^4$ ($\Delta T = 20\,\mathrm{K}$) for $V/V_0 = 0.8$ and $\Gamma = 2.0$. Schematic of the trajectory of the particles forming the coherent structure is illustrated in the first panel superimposed on the same images indicated in (i). The point "A" indicates the position of the trajectory where the coherent structure locating closest to the free surface near the heated disk, and the particles travel along the positions on the trajectory in the alphabetical order. Note that this result was obtained in the different experimental run shown in Fig. 5.

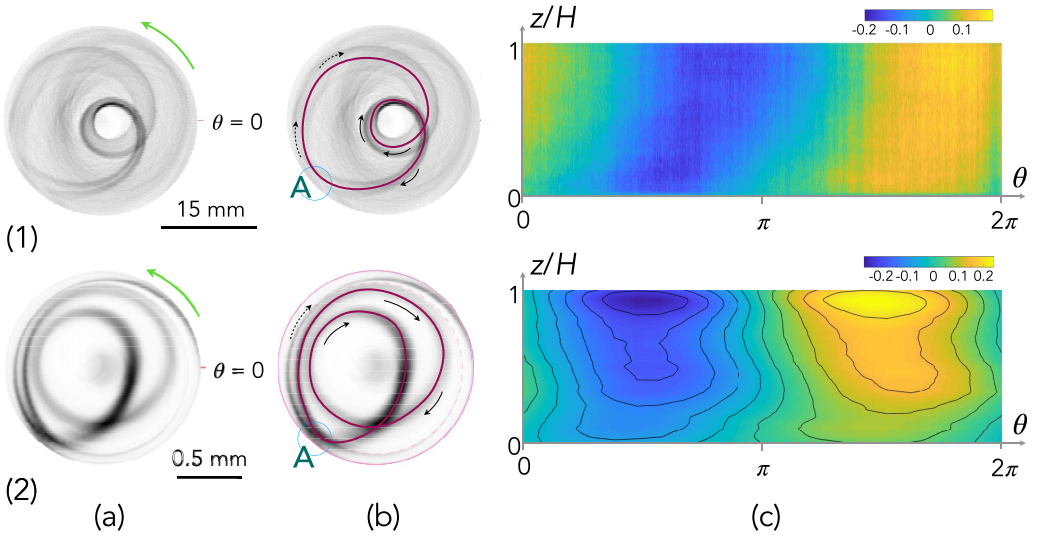


FIG. 7. (a) Coherent structure in rotating frame of reference observed through hot disk, (b) its schematics, and (c) temperature-deviation distribution over free surface for (1) microgravity- and (2) terrestrial experiments. The coherent-structure images are obtained by integrating the particle images for (1) four fundamental periods or 131.4 s and for (2) ten fundamental periods or 3.8 s. Arrows in row (a) indicate the direction of the traveling wave. Solid and dashed arrows in row (b) indicate the upward ($\partial z/\partial t \geqslant 0$) and downward ($\partial z/\partial t \leqslant 0$) motions of the particles forming the PAS, respectively. Circle in row (b) illustrates the position "A" where the coherent structure seems locating closest to the free surface, as shown in Figs. 4 and 6.

under $\mathrm{Bd} = 0.34$ in the slender liquid bridge of $\Gamma = 2.0$, whose 'net' aspect ratio is greater than 2.0; such feature is supported by the results that oscillatory thermal flows emerge with smaller $m$ by increasing $\Gamma$ under a fixed $V/V_0$ [3,6,7,12] and by decreasing $V/V_0$ under a fixed $\Gamma$ [70].

### C. Coherent structures in rotating frame of reference

We now focus on the spatial correlation of the particles on the coherent structure and the thermal wave over the free surface. Figure 7 illustrates (a) the coherent structure in the rotating frame of reference observed through the hot disk, (b) its schematics, and (c) the temperature-deviation distribution over the free surface for (1) the microgravity- and (2) the terrestrial experiments. The coherent-structure images are obtained by integrating the particle images for (1) four fundamental periods or 131.4 s and for (2) ten fundamental periods or 3.8 s. Arrows in row (a) indicate the direction of the traveling wave. It must be noted again here that frame (a) for (1) the microgravity experiment does not indicate the "top" view; because of the inclination of the incident angle of the camera, one cannot obtain images without broadening the width of the particle trajectories by accumulating the frames. In frame (b), we put the arrows indicating the motion of the particles on the PAS; solid and dashed arrows in row (b) indicate the upward ($\partial z/\partial t \geqslant 0$) and downward ($\partial z/\partial t \leqslant 0$) motions of the particles forming the PAS, respectively. Note that the positive and negative sign for the particle motion is not perfectly reproduced as aforementioned. The spatial distribution of the temperature deviation over the free surface is reconstructed by following the procedures in the previous studies [10,44,63]: We accumulate the temporal distribution of the surface temperature along a monitoring line normal to the both end disks at a fixed azimuthal position, and convert the temporal variation to the spatial variation against the azimuthal position by considering the constant propagation speed of the traveling wave. For both cases there exist a pair of relatively hotter ($\widehat{T} > 0$) and colder ($\widehat{T} < 0$) regions over the free surface. We convince ourselves

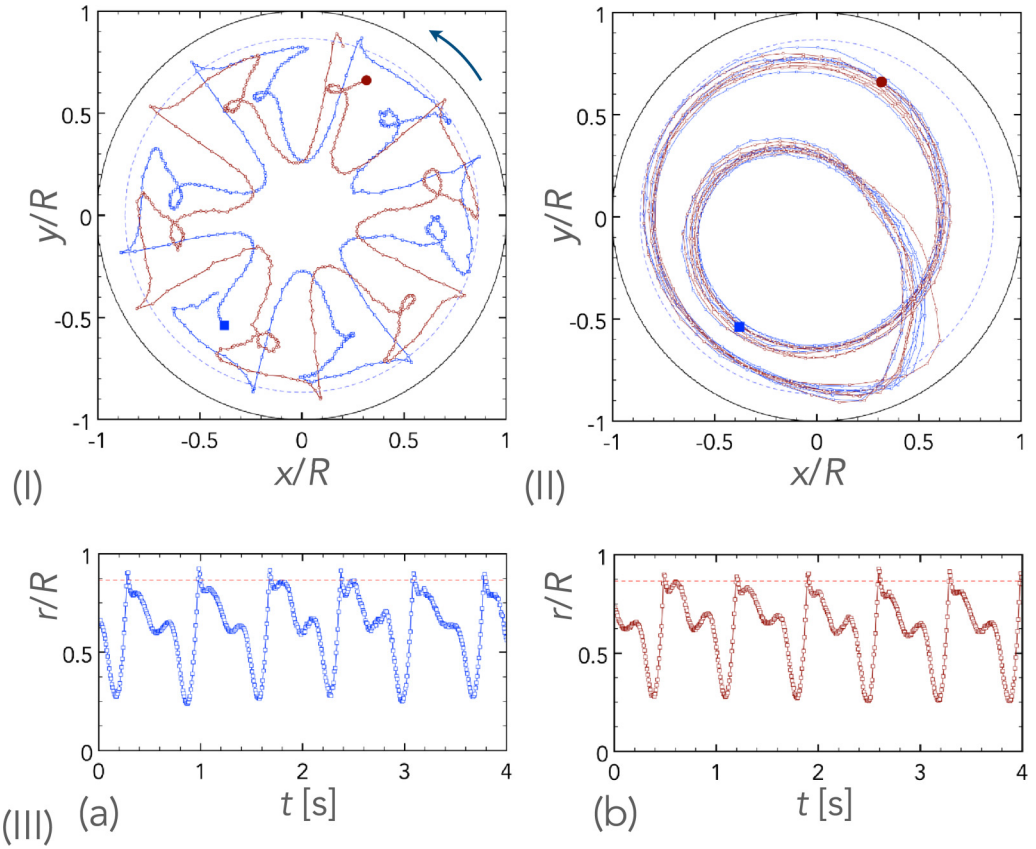


FIG. 8. Typical motion by two different particles forming the PAS in (I) the laboratory frame and (II) the rotating frame of reference observed from above for 3.992 s with a constant interval of 1/125 s, and (III) their temporal variations of radial positions. Two large filled marks (square and circle) in frames (I) and (II) indicate the initial positions of the particles in the observation period. Panels (a) and (b) in frame (III) indicate the temporal variations of the particle whose initial position is illustrated by the filled square (in blue) and (b) the particle by the filled circle (in red), respectively. The circles by solid line and dashed line in frames (I) and (II) show the periphery of the top rod of 0.75 mm in radius and the averaged position of the free surface of minimum radius, respectively. An arrow in frame (I) indicates the azimuthal direction of the thermal wave over the free surface or the azimuthal direction of the PAS rotation.

that we realize the thermal flow field of the azimuthal wave number $m = 1$. In the case of (1) the microgravity experiment, the thermal wave seems to propagate from the heated disk to the cooled one with an inclined propagation angle. In the case of (2) the terrestrial experiment, however, the thermal wave seems to propagate almost parallel to the $z$ axis. These are the typical features of the oscillatory thermal flow of the HTW(a) or HTW(a′) and that of the HTW(b), respectively [68], as aforementioned. We find that the coherent structure of $m = 1$ with a spiral structure around the particle depletion zone is realized even though the thermal flow field has different basic flow structure induced by the HTW instability. The coherent structures in the both cases are the same as the one realized in the previous terrestrial experiment [35] and by the numerical simulation [36]. The both have similar azimuthal positions at $\theta \sim 1.3\pi$ rad where the coherent structure reaches closest to the free surface. In (1) the microgravity experiment this position corresponds where the temperature deviation is almost neutral, and in (2) the terrestrial experiment this corresponds where the hotter region is located, which is similar to the result for the SL1- and SL2-PASs of $m = 3$ [10];

Toyama *et al.* [10] indicated that the correlation between the position where the coherent structure comes closest to the free surface and the temperature deviation over the free surface becomes different by varying Pr, and considered that the correlation is defined by the flow field inside the liquid bridge induced by the thermocapillary effect. It is indispensable to obtain the highly resolved thermal flow field inside the liquid bridge and the distributions of the particles to form the coherent structure.

To illustrate the correlation between the PAS of $m = 1$ with a spiral structure and the individual particle behavior, typical motions of two different particles forming the PAS in (I) the laboratory frame and (II) the rotating frame of reference observed from above are illustrated in Fig. 8. The circle by solid line shows the periphery of the top rod of 0.75 mm in radius. The concentric circle by dashed line indicates the averaged position of the free surface of minimum radius. The particles' positions are depicted from the successive images of the top view for 3.992 s with a constant interval of 1/125 s. An arrow in frame (I) indicates the azimuthal direction of the thermal wave over the free surface or the azimuthal direction of the PAS rotation. One finds two large filled marks (square and circle) in frames (I) and (II); these are the positions of the particles detected in the first image of the successive data. That is, these are the initial positions of two different particles in the observation period. The temporal variations of their radial positions are shown in frame (III): (a) the particle whose initial position is illustrated by the filled square (in blue) and (b) the particle by the filled circle (in red). The particles forming the PAS travel in the liquid bridge regularly and periodically, which is also recognized in frame (I). The turnover time of each particle is almost constant at 0.676 s or 1.48 Hz. The frequency ratio against the PAS rotation or the thermal wave propagation in the azimuthal direction, $f_p/f_{HTW}$, is about 0.56. This ratio is almost one-third of that for the PAS of $m = 3$ [17]. When one tracks the particles in frame (II), the rotating frame of reference, one finds that the two-dimensional conformation of the PAS is surely reconstructed. The trajectories of the particles forming the PAS in the interior region of the liquid bridge are densely located. In other words, the particles forming the PAS travel along a narrow path in the liquid-bridge interior. The trajectories from the central region toward the free surface, on the contrary, are rather scattered as seen in Fig. 7 (2). It has been indicated that the PAS as the coherent structure is formed by the particles attracted to the Kolmogorov-Arnold-Moser (KAM) tori within the closed flow field [17,55]. This experimental result implies the shape of the KAM of $m = 1$; the torus with a spiral structure might be broadened near the heated disk from the center of the liquid bridge toward the free surface. Further research be needed to lead comprehensive understandings of the correlation between the flow field and the coherent structures by tiny particles.

To illustrate the morphology of the spiral structure in the interior region of the liquid bridge, we monitor the variation of the particle distribution in the rotating frame of reference and in the laboratory frame as conducted for the PAS of $m = 3$ [17]. Figure 9 illustrates the variation of particle distribution in the top view for $\mathrm{Ma} = 2.3 \times 10^4$ (or $\Delta T = 24\,\mathrm{K}$) in (a) the rotating frame of reference and in (b) the laboratory frame as a function of $V/V_0$ in liquid bridge of $\Gamma = 2.0$ under normal gravity. Each frame is obtained by accumulating the particle images for five fundamental cycles. Note that the dashed circle in each frame indicates the minimum position of the concave free surface. In row (c), the side-view snapshots of the liquid bridge are shown. In the liquid bridge of $V/V_0 = 0.73$ and 0.75, one finds a rather vague structure in the interior region of the liquid bridge is apparently formed. This is a precursor of the coherent structure with a spiral structure. It is found that the particles disperse not only on the PAS but also in the rest region inside the liquid bridge. Thus, the boundaries of the particles existing region is not apparently distinguished in the accumulated image in the laboratory frame. By increasing $V/V_0$, the whole coherent structure is rigidly formed ($V/V_0 = 0.76$ and 0.79). Once the coherent structure is rigidly formed, the boundaries of the particle distributions become clearly distinguishable in the laboratory frame; one finds several coaxial circular bands of the particles. The darker regions correspond to the projected area where more particles travel, and vice versa. By further increasing $V/V_0$, the width of the coherent structure becomes widened and vague ($V/V_0 = 0.84$), and finally no coherent structures are detected ($V/V_0 = 0.89$). One finds the formation of the coherent structure is sensitive not only to

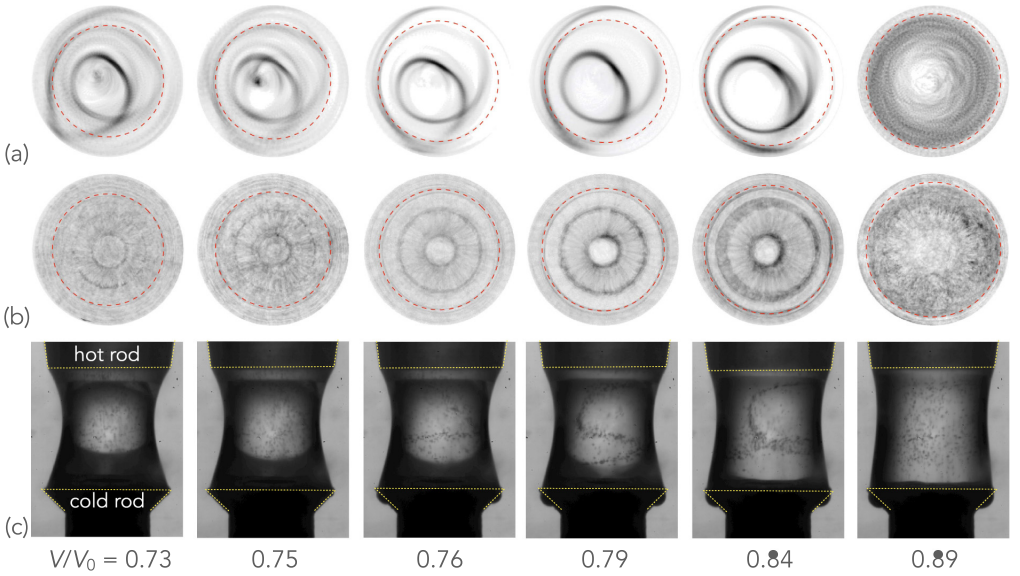


FIG. 9. Variation of particle distribution in top view for $\mathrm{Ma} = 2.3 \times 10^4$ ($\Delta T = 24\,\mathrm{K}$); in (a) rotating frame of reference and in (b) laboratory frame as a function of $V/V_0$ in liquid bridge of $\Gamma = 2.0$ under normal gravity. Each frame for top views is obtained by accumulating the particle images for five fundamental cycles. Dashed circle in each frame indicates the minimum position of the concave free surface. The azimuthal direction of the PAS for each case is counterclockwise. Row (c) illustrates the side-view snapshots of the liquid bridge.

$\Delta T$ or Ma [17] but also to $V/V_0$. The shape of the spiral structure in the interior region of the liquid bridge is rather less sensitive to $V/V_0$; one finds no drastic variation of the spiral structure against it except its size.

To illustrate the size variation of the spiral structure against $V/V_0$, we measure the maximum and minimum distances in $r$ of the spiral structure from the liquid-bridge center as indicated in Fig. 10 (1). Frames (a) and (b) in column (1) show the definition of the maximum distance $R_s^{(\max)}$ and minimum one $R_s^{(\min)}$ with the top view of the accumulated particle images in (a) the rotating frame of reference and in (b) the laboratory frame for $V/V_0 = 0.68$, respectively. Here the accumulated particle images are obtained under $\mathrm{Ma} = 1.9 \times 10^4$. Note that $R_s^{(\min)}$ corresponds to $R_{\mathrm{PAS}}$ defined in Ref. [17]. Especially in the top view in the laboratory frame, these two distances are clearly indicated once the coherent structure is rigidly formed. Column (2) illustrates the variations of $R_s^{(\max)}$ (square) and $R_s^{(\min)}$ (circle) against $V/V_0$ for $\mathrm{Ma} = 1.9 \times 10^4$ (or $\Delta T = 20\,\mathrm{K}$) and $2.3 \times 10^4$ (or $\Delta T = 24\,\mathrm{K}$). It is found that $R_s^{(\max)}$ increases as $V/V_0$ increases, whereas $R_s^{(\min)}$ decreases. That is, as $V/V_0$ increases, the particles approach closer to the free surface when they rise from the bottom, whereas the particles travel nearer the liquid-bridge center when they turn their direction toward the free surface. It is also found that $R_s^{(\max)}$ is almost the same for Ma, but that $R_s^{(\min)}$ differs by varying Ma. By considering that the coherent structure exhibits similar structure to the KAM tori in the case of the PAS of $m = 1$ [36] as well as the PAS of $m = 3$ [17,18,31,55], such information is directly connected to the KAM tori realized in the tall liquid bridges. Further research is deserved to illustrate the correlation between the KAM tori and the coherent structures with a spiral structure, as indicated for the coherent structures of $m = 1$ without the spiral structure in the liquid bridge of $\mathrm{Pr} = 68$ [39,40]. It would also be indispensable to accumulate information on the effect of St on the formation of the coherent structures, although it would be a challenge especially under the normal gravity condition because of the severe limitation of the liquid-bridge size.

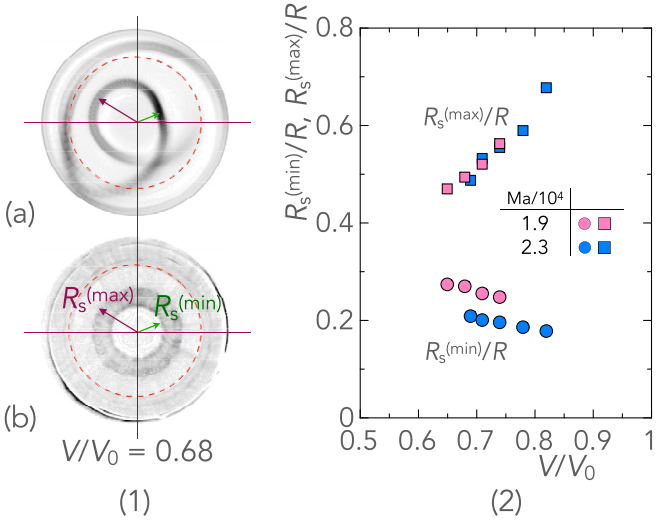


FIG. 10. Maximum and minimum distances of spiral structure in $r$ direction, $R_s^{(max)}$ and $R_s^{(min)}$, respectively, in liquid bridge of $\Gamma = 2.0$ under normal gravity. (1) Definition of $R_s^{(min)}$ and $R_s^{(max)}$ with the particle distribution (a) in the rotating frame of reference and (b) in the laboratory frame for the liquid bridge of $V/V_0 = 0.68$ for $\mathrm{Ma} = 1.9 \times 10^4$ ($\Delta T = 20\,\mathrm{K}$), and (2) their variation against $V/V_0$ under $\mathrm{Ma} = 1.9 \times 10^4$ ($\Delta T = 20\,\mathrm{K}$) and $\mathrm{Ma} = 2.3 \times 10^4$ ($\Delta T = 24\,\mathrm{K}$). Dashed circle in each frame indicates the minimum position of the concave free surface.

## IV. CONCLUDING REMARKS

The coherent structures by low-Stokes-number particles suspended in half-zone thermocapillary liquid bridges of high Prandtl number are investigated via microgravity and terrestrial experiments. We pay our special attention to the particle accumulation structure (PAS) after Schwabe *et al.* [1] of $m = 1$ in azimuthal wave number emerged in the traveling-wave-type time-dependent "oscillatory" convection. We successfully realize the coherent structures of $m = 1$ in a large-scale liquid bridge in the on-orbit experiment within the project so-called the "Dynamic Surf." Those are the first examples to steadily produce the PAS of $m = 1$ under long-duration microgravity conditions. We also realize the coherent structures of $m = 1$ successfully in small-size liquid bridges of various volume ratio $V/V_0$ in the terrestrial experiments with a test liquid of Pr higher than that in Ref. [12].

We find that the particles form the closed path with a spiral structure in tall or high-aspect-ratio liquid bridges under both micro- and normal gravity conditions: The coherent structures of $m = 1$ are stably realized in the liquid bridge of $\mathrm{Pr} = 113.5$ under $\Gamma = 1.0$ and $V/V_0 = 0.95$ in the microgravity experiments, whereas are successfully realized in the liquid bridges of $\mathrm{Pr} = 28.6$ under $\Gamma = 2.0$ and $V/V_0$ in a range $0.6 \leqslant V/V_0 \leqslant 0.8$ in the terrestrial experiments.

We evaluate their formation process by applying the accumulation measure $K(t)$, and indicate that the formation time of the structure is of the order of a thermal diffusion time regardless the gravitational acceleration and the Pr of the test liquid. We illustrate the top- and side views of the particles forming the coherent structures under developed stage accompanying with the surface temperature variation due to the hydrothermal wave instability. The spatial correlation between the coherent structure and the thermal wave over the free surface is illustrated in the rotating frame of reference. It is found that the particles exhibits the closed path with a spiral structure in the interior region of the liquid bridge as indicated in Ref. [35] despite that the thermal flow structure is different under the normal- and microgravity conditions.

We indicate how the PAS of $m = 1$ with a spiral structure is configurated by the individual particles via particle tracking; typical motion of different particles forming the PAS is illustrated in the laboratory frame and the rotating frame of reference observed from above. We find that

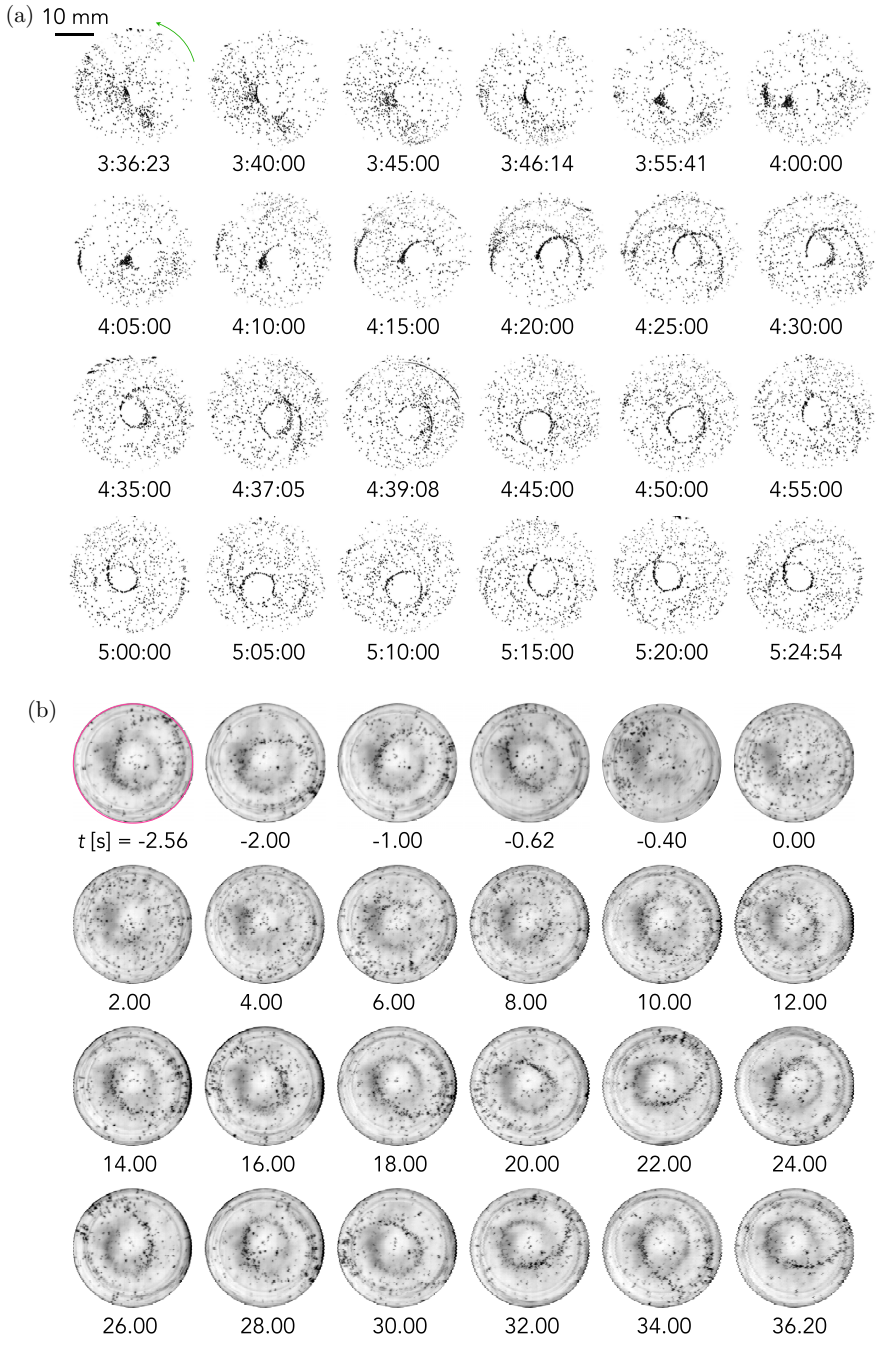


FIG. 11. Time series of the particle image observed from above via (a) microgravity- and (b) terrestrial experiment: (a) $\mathrm{Ma} = 1.30 \times 10^4$ ($\Delta T = 8.2\,\mathrm{K}$ and $\epsilon = 0.8$) in the liquid bridge of $V/V_0 = 0.95$ and $\Gamma = 1.0$, and (b) $\mathrm{Ma} = 1.9 \times 10^4$ ($\Delta T = 20\,\mathrm{K}$) in the liquid bridge of $V/V_0 = 0.8$ for $\Gamma = 2.0$. The azimuthal direction of the PAS and the thermal wave over the free surface due to the hydrothermal wave instability is counterclockwise. Note for (b) the terrestrial experiment that the azimuthal direction of the PAS rotation changes from the counterclockwise to the clockwise after the disturbances added in the period of $-1.1\,\mathrm{s} \leqslant t \leqslant 0\,\mathrm{s}$.

the particles forming the PAS travel along a narrow path in the liquid-bridge interior, whereas the trajectories from the central region toward the free surface are rather scattered.

To illustrate the morphology of the spiral structure in the interior region of the liquid bridge, we monitor the variation of the particle distribution in the rotating frame of reference and in the laboratory frame. We measure the maximum and minimum radii of spiral structure, $R_s^{(\max)}$ and $R_s^{(\min)}$, in the liquid bridge of $\Gamma = 2.0$ under normal gravity against $V/V_0$.

As for the existing condition in $\epsilon$, it is found that the PAS of $m = 1$ with a spiral structure emerges at much lower $\epsilon$ ($\epsilon = 0.18$) under the microgravity condition than the PAS of $m = 3$ on the ground ($2 \lesssim \epsilon \lesssim 4$) [7].

Further research is needed for illustrating the precise three-dimensional structure of the coherent structure, which reflect the Kolmogorov-Arnold-Moser (KAM) tori realized in the liquid bridges, and for exploring the existing condition of the PAS of $m = 1$.

## ACKNOWLEDGMENTS

We acknowledge Dr. H. Kawamura (emeritus professor, Tokyo University of Science, Japan) for fruitful discussion. This work was partially supported from the Japan Society for the Promotion of Science (JSPS) by Grant-in-Aid for Challenging Research (Exploratory) (Grant No. 20K20977).

## APPENDIX A: PARTICLE IMAGES OF THE COHERENT STRUCTURES UNDER MICRO- AND NORMAL GRAVITY

Figure 11 illustrates typical examples of the long-period particle behaviors forming the coherent structure of $m = 1$ obtained (a) in the microgravity and (b) in the normal gravity experiments. Each panel illustrates the particle behaviors in the laboratory frame. Fundamental period of the oscillatory convection is of (a) 32.85 s and (b) 0.38 s. Note for (b) the terrestrial experiment that the PAS of $m = 1$ with a spiral structure is once fully established for $t < -1.1$ s. At $t = -1.1$ s we put a disturbance to the free surface by blowing a tiny amount of the air through the external shield. We then stop blowing at $t = 0$ s. Note that the azimuthal direction of the rotation after the disturbances varies from the counterclockwise to the clockwise.

## APPENDIX B: TYPES OF THERMAL-FLOW FIELD PREDICTED BY LSA

Figure 12(1) illustrates the neutral curves predicted by the linear stability analysis (LSA) by Fujimoto *et al.* [68] for the straight liquid bridge of Pr = 28.6 under Bd = 0.34 (in red) and 0

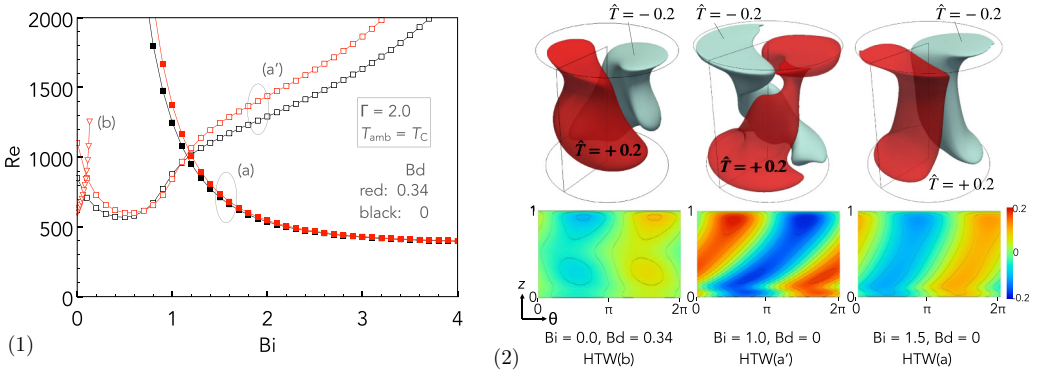


FIG. 12. Predictions by linear stability analysis (LSA) for the straight liquid bridge of Pr = 28.6 [68]: (1) neutral curves under Bd = 0.34 (in red) and 0 (in black), (2) typical examples of distributions of isosurfaces of $\widehat{T} = \pm 0.2$ inside liquid bridge (top) and of temperature deviation $\widehat{T}$ over free surface for different types of HTW. The eigenfunctions of the induced thermal flow fields are named as the HTW(b) for small Bi (left), the HTW(a′) for moderate Bi (middle), and the HTW(a) for large Bi (right). The azimuthal traveling direction of the thermal wave over the free surface is counterclockwise for all cases in this figure.

(in black). Column (2) illustrates the distributions of the isosurfaces of $\widehat{T} = \pm 0.2$ inside the liquid bridge (top) and of the temperature deviation $\widehat{T}$ over the free surface for different types of the HTW. The eigenfunctions of the induced thermal flow fields are named the HTW(b) for small Bi (left), the HTW(a′) for moderate Bi (middle), and the HTW(a) for large Bi (right).


[1] D. Schwabe, P. Hintz, and S. Frank, New features of thermocapillary convection in floating zones revealed by tracer particle accumulation structure (PAS), Microgravity Sci. Technol. **9**, 163 (1996).

[2] J.-J. Xu and S. H. Davis, Instability of capillary jets with thermocapillarity, J. Fluid Mech. **161**, 1 (1985).

[3] F. Preisser, D. Schwabe, and A. Scharmann, Steady and oscillatory thermocapillary convection in liquid columns with free cylindrical surface, J. Fluid Mech. **126**, 545 (1983).

[4] M. Wanschura, V. M. Shevtsova, H. C. Kuhlmann, and H. J. Rath, Convective instability mechanisms in thermocapillary liquid bridges, Phys. Fluids **7**, 912 (1995).

[5] J. Leypoldt, H. C. Kuhlmann, and H. J. Rath, Three-dimensional numerical simulation of thermocapillary flows in cylindrical liquid bridges, J. Fluid Mech. **414**, 285 (2000).

[6] I. Ueno, S. Tanaka, and H. Kawamura, Oscillatory and chaotic thermocapillary convection in a half-zone liquid bridge, Phys. Fluids **15**, 408 (2003).

[7] S. Tanaka, H. Kawamura, I. Ueno, and D. Schwabe, Flow structure and dynamic particle accumulation in thermocapillary convection in a liquid bridge, Phys. Fluids **18**, 067103 (2006).

[8] T. Ogasawara, K. Motegi, T. Hori, and I. Ueno, Secondary instability induced by thermocapillary effect in half-zone liquid bridge of high Prandtl number fluid, Mechan. Engine. Lett. **5**, 19-00014 (2019).

[9] Y. Niigaki and I. Ueno, Formation of particle accumulation structure (PAS) in half-zone liquid bridge under an effect of thermo-fluid flow of ambient gas, Trans. JSASS (Japan Soc. for Aeronaut. Space Sci. Aerospace Technology) **10**, Ph33 (2012).

[10] A. Toyama, M. Gotoda, T. Kaneko, and I. Ueno, Existence conditions and formation process of second type of spiral loop particle accumulation structure (SL-2 PAS) in half-zone liquid bridge, Microgravity Sci. Technol. **29**, 263 (2017).

[11] H. Kawamura, K. Nishino, S. Matsumoto, and I. Ueno, Report on microgravity experiments of Marangoni convection aboard International Space Station, J. Heat Transfer **134**, 031005 (2012).

[12] D. Schwabe, A. I. Mizev, M. Udhayasankar, and S. Tanaka, Formation of dynamic particle accumulation structures in oscillatory thermocapillary flow in liquid bridges, Phys. Fluids **19**, 072102 (2007).

[13] I. Ueno, Y. Abe, K. Noguchi, and H. Kawamura, Dynamic particle accumulation structure (PAS) in half-zone liquid bridge—Reconstruction of particle motion by 3D PTV, Adv. Space Res. **41**, 2145 (2008).

[14] Y. Abe, I. Ueno, and H. Kawamura, Dynamic particle accumulation structure due to thermocapillary effect in noncylindrical half-zone liquid bridge, Ann. N.Y. Acad. Sci.Interdisciplinary Transport Phenomena, **1161**, 240 (2009).

[15] D. E. Melnikov, T. Watanabe, T. Matsugase, I. Ueno, and V. Shevtsova, Experimental study on formation of particle accumulation structures by a thermocapillary flow in a deformable liquid column, Microgravity Sci. Technol. **26**, 365 (2014).

[16] M. Gotoda, T. Sano, T. Kaneko, and I. Ueno, Evaluation of existence region and formation time of particle accumulation structure (PAS) in half-zone liquid bridge, Eur. Phys. J.: Spec. Top. **224**, 299 (2015).

[17] M. Gotoda, A. Toyama, M. Ishimura, T. Sano, M. Suzuki, T. Kaneko, and I. Ueno, Experimental study of coherent structures of finite-size particles in thermocapillary liquid bridges, Phys. Rev. Fluids **4**, 094301 (2019).

[18] T. Oba, A. Toyama, T. Hori, and I. Ueno, Experimental study on behaviors of low-stokes number particles in weakly chaotic structures induced by thermocapillary effect within a closed system with a free surface, Phys. Rev. Fluids **4**, 104002 (2019).

[19] K. Nishino, T. Yano, H. Kawamura, S. Matsumoto, I. Ueno, and M. K. Ermakov, Instability of thermocapillary convection in long liquid bridges of high Prandtl number fluids in microgravity, J. Cryst. Growth **420**, 57 (2015).

[20] I. Ueno, Experimental study on coherent structures by particles suspended in half-zone thermocapillary liquid bridges: Review, Fluids **6**, 105 (2021).
[21] M. Takatsuka, S. Tanaka, I. Ueno, and H. Kawamura, Dynamic particle accumulation structure of Marangoni convection in liquid bridge. 2. Numerical simulation, in *Proceedings of the Thermal Engineering Conference (in Japanese)* (Japan Society for Mechanical Engineers, 2002), pp. 307–308.
[22] T. Seki, S. Tanaka, and H. Kawamura, Numerical simulation of particle accumulatoin structure in oscillatory thermocapillary convection of a liquid bridge, in *Proceedings of the Thermal Engineering Conference (in Japanese)* (Japan Society for Mechanical Engineers, 2005), pp. 169–170.
[23] D. E. Melnikov, D. O. Pushkin, and V. M. Shevtsova, Accumulation of particles in time-dependent thermocapillary flow in a liquid bridge: Modeling and experiments, Eur. Phys. J.: Spec. Top. **192**, 29 (2011).
[24] H. C. Kuhlmann and F. H. Muldoon, Particle-accumulation structures in periodic free-surface flows: Inertia versus surface collisions, Phys. Rev. E **85**, 046310 (2012).
[25] M. Lappa, On the variety of particle accumulation structures under the effect of g-jitters, J. Fluid Mech. **726**, 160 (2013).
[26] M. Lappa, Assessment of the role of axial vorticity in the formation of particle accumulation structures in supercritical Marangoni and hybrid thermocapillary-rotation-driven flows, Phys. Fluids **25**, 012101 (2013).
[27] D. E. Melnikov, D. O. Pushkin, and V. M. Shevtsova, Synchronization of finite-size particles by a traveling wave in a cylindrical flow, Phys. Fluids **25**, 092108 (2013).
[28] F. H. Muldoon and H. C. Kuhlmann, Coherent particulate structures by boundary interaction of small particles in confined periodic flows, Physica D **253**, 40 (2013).
[29] F. H. Muldoon and H. C. Kuhlmann, Different particle-accumulation structures arising from particle-boundary interactions in a liquid bridge, Int. J. Multiphase Flow **59**, 145 (2014).
[30] F. H. Muldoon and H. C. Kuhlmann, Origin of particle accumulation structures in liquid bridges: Particle-boundary-interactions versus inertia, Phys. Fluids **28**, 073305 (2016).
[31] F. Romanò and H. C. Kuhlmann, Finite-size lagrangian coherent structures in thermocapillary liquid bridges, Phys. Rev. Fluids **3**, 094302 (2018).
[32] F. Romanò and H. C. Kuhlmann, Finite-size coherent structures in thermocapillary liquid bridges, Int. J. Microgravity Sci. Appl. **36**, 360201 (2019).
[33] P. Capobianchi and M. Lappa, Particle accumulation structures in noncylindrical liquid bridges under microgravity conditions, Phys. Rev. Fluids **5**, 084304 (2020).
[34] S. Yazawa and H. Kawamura, Experiment of Marangoni convection in a liquid bridge with a low to medium aspect ratio, in *Proceedings of the National Heat Transfer Symposium of Japan (in Japanese)* (2010), p. SP409.
[35] Y. Sasaki, S. Tanaka, and H. Kawamura, Particle accumulation structure in thermocapillary convection of small liquid bridge, in *Proceedings of the 6th Japan/China Workshop on Microgravity Sciences* (2005).
[36] P. Capobianchi and M. Lappa, On the influence of gravity on particle accumulation structures in high aspect-ratio liquid bridges, J. Fluid Mech. **908**, A29 (2021).
[37] P. Capobianchi and M. Lappa, Particle accumulation structures in a 5 cSt silicone oil liquid bridge: New data for the preparation of the JEREMI experiment, Microgravity Sci. Technol. **33**, 31 (2021).
[38] I. Barmak, F. Romanò, and H. C. Kuhlmann, Particle accumulation in high-Prandtl-number liquid bridges, Proc. Appl. Math. Mech. **19**, e201900058 (2019).
[39] I. Barmak, F. Romanò, P. K. Kannan, and H. C. Kuhlmann, Coherent particle structures in high-Prandtl-number liquid bridges, Microgravity Sci. Technol. **33**, 19 (2021).
[40] I. Barmak, F. Romanò, and H. C. Kuhlmann, Finite-size coherent particle structures in high-Prandtl-number liquid bridges, Phys. Rev. Fluids **6**, 084301 (2021).
[41] D. Schwabe, Hydrothermal wave in a liquid bridge with aspect ratio near the Rayleigh limit under microgravity, Phys. Fluids **17**, 112104 (2005).
[42] D. Schwabe, Hydrodynamic instabilities under microgravity in a differentially heated long liquid bridge with aspect ratio near the Rayleigh-limit: Experimental results, Adv. Space Res. **36**, 36 (2005).

[43] T. Yano, K. Nishino, H. Kawamura, I. Ueno, S. Matsumoto, M. Ohnishi, and M. Sakurai, Space experiment on the instability of Marangoni convection in large liquid bridge—MEIS-4: Effect of Prandtl number, J. Phys.: Conf. Ser. **327**, 012029 (2011).
[44] F. Sato, I. Ueno, H. Kawamura, K. Nishino, S. Matsumoto, M. Ohnishi, and M. Sakurai, Hydrothermal wave instability in a high-aspect-ratio liquid bridge of Pr >200, Microgravity Sci. Technol. **25**, 43 (2013).
[45] T. Yano, K. Nishino, H. Kawamura, I. Ueno, and S. Matsumoto, Instability and associated roll structure of Marangoni convection in high Prandtl number liquid bridge with large aspect ratio, Phys. Fluids **27**, 024108 (2015).
[46] T. Matsugase, I. Ueno, K. Nishino, M. Ohnishi, M. Sakurai, S. Matsumoto, and H. Kawamura, Transition to chaotic thermocapillary convection in a half zone liquid bridge, Int. J. Heat Mass Transf. **89**, 903 (2015).
[47] T. Yano, K. Nishino, S. Matsumoto, I. Ueno, A. Komiya, Y. Kamotani, and N. Imaishi, Report on microgravity experiments of dynamic surface deformation effects on Marangoni instability in high-Prandtl-number liquid bridges, Microgravity Sci. Technol. **30**, 599 (2018).
[48] T. Yano, K. Nishino, S. Matsumoto, I. Ueno, A. Komiya, Y. Kamotani, and N. Imaishi, Overview of "Dynamic Surf" project in Kibo—Dynamic behavior of large-scale thermocapillary liquid bridges in microgravity, Int. J. Microgravity Sci. Appl. **35**, 350102 (2018).
[49] T. Yano, K. Nishino, I. Ueno, S. Matsumoto, and Y. Kamotani, Sensitivity of hydrothermal wave instability of Marangoni convection to the interfacial heat transfer in long liquid bridges of high Prandtl number fluids, Phys. Fluids **29**, 044105 (2017).
[50] S. Matsumoto, K. Nishino, I. Ueno, T. Yano, and H. Kawamura, Marangoni experiment in space, Int. J. Microgravity Sci. Appl. **31**, S51 (in Japanese) (2014).
[51] Y. Fukuda, T. Ogasawara, S. Fujimoto, T. Eguchi, K. Motegi, and I. Ueno, Thermal-flow patterns of $m = 1$ in thermocapillary liquid bridges of high aspect ratio with free-surface heat transfer, Int. J. Heat Mass Transf. **173**, 121196 (2021).
[52] Shin-Etsu Chemical Company Limited, Technical Data: Silicone fluid KF96 Performance Test Results, Tech. Rep. (Shin-Etsu Chemical Co., Ltd., 2014).
[53] T. Yano, K. Nishino, H. Kawamura, I. Ueno, S. Matsumoto, M. Ohnishi, and M. Sakurai, 3-D PTV measurement of Marangoni convection in liquid bridge in space experiment, Exp. Fluids **53**, 9 (2012).
[54] T. Takakusagi and I. Ueno, Flow patterns induced by thermocapillary effect and resultant structures of suspended particles in a hanging droplet, Langmuir **33**, 13197 (2017).
[55] H. C. Kuhlmann, R. V. Mukin, T. Sano, and I. Ueno, Structure and dynamics of particle-accumulation in thermocapillary liquid bridges, Fluid Dyn. Res. **46**, 041421 (2014).
[56] Japan Aerospace Exploration Agency (JAXA), Kibo Handbook (2007).
[57] J. Shiomi, M. Kudo, I. Ueno, H. Kawamura, and G. Amberg, Feedback control of oscillatory thermocapillary convection in a half-zone liquid bridge, J. Fluid Mech. **496**, 193 (2003).
[58] H. Kawamura and I. Ueno, Review on thermocapillary convection in a half-zone liquid bridge with high Pr fluid: Onset of oscillatory convection, transition of flow regimes, and particle accumulation structure, in *Surface Tension-Driven Flows and Applications*, edited by R. Savino (Research Signpost, Kerala, India, 2006), Chap. 1, pp. 1–24.
[59] E. Hofmann and H. C. Kuhlmann, Particle accumulation on periodic orbits by repeated free surface collisions, Phys. Fluids **23**, 072106 (2011).
[60] D. Schwabe, A. Mizev, S. Tanaka, and H. Kawamura, Particle accumulation structures in time-dependent thermocapillary flow in a liquid bridge under microgravity, Microgravity Sci. Technol. **18**, 117 (2006).
[61] J.-J. Xu and S. H. Davis, Convective thermocapillary instabilities in liquid bridges, Phys. Fluids **27**, 1102 (1984).
[62] I. I. Ryzhkov, Thermocapillary instabilities in liquid bridges revisited, Phys. Fluids **23**, 082103 (2011).
[63] I. Ueno, H. Kawasaki, T. Watanabe, K. Motegi, and T. Kaneko, Hydrothermal-wave instability and resultant flow patterns induced by thermocapillary effect in a half-zone liquid bridge of high aspect ratio, *Proceedings of the 15th International Heat Transfer Conference (IHTC-15) ihtc15* (2014).
[64] M. K. Smith and S. H. Davis, Instabilities of dynamic thermocapillary liquid layers. Part 1. Convective instabilities, J. Fluid Mech. **132**, 119 (1983).

[65] R. J. Riley and G. P. Neitzel, Instability of thermocapillary-buoyancy convection in shallow layers. Part 1. Characterization of steady and oscillatory instabilities, J. Fluid Mech. **359**, 143 (1998).

[66] H. Kawamura, E. Tagaya, and Y. Hoshino, A consideration on the relation between the oscillatory thermocapillary flow in a liquid bridge and the hydrothermal wave in a thin liquid layer, Int. J. Heat Mass Transf. **50**, 1263 (2007).

[67] T. Watanabe, T. Takakusagi, I. Ueno, H. Kawamura, K. Nishino, M. Ohnishi, M. Sakurai, and S. Matsumoto, Terrestrial and microgravity experiments on onset of oscillatory thermocapillary-driven convection in hanging droplets, Int. J. Heat Mass Transf. **123**, 945 (2018).

[68] S. Fujimoto, T. Ogasawara, A. Ota, K. Motegi, and I. Ueno, Effect of heat loss on hydrothermal wave instability in half-zone liquid bridges of high Prandtl number fluid, Int. J. Microgravity Sci. Appl. **36**, 360204 (2019).

[69] Y. Kamotani, L. Wang, S. Hatta, A. Wang, and S. Yoda, Free surface heat loss effect on oscillatory thermocapillary flow in liquid bridges of high Prandtl number fluids, Int. J. Heat Mass Transf. **46**, 3211 (2003).

[70] T. Yano, K. Maruyama, T. Matsunaga, and K. Nishino, Effect of ambient gas flow on the instability of Marangoni convection in liquid bridges of various volume ratios, Int. J. Heat Mass Transf. **99**, 182 (2016).